Vibrational spectroscopy and DFT calculations of 1,3-dibromo-2,4,6-trimethylbenzene: Anharmonicity, coupling and methyl group tunneling

Soraya Zeroual, Jean Meinnel, Andrzej Lapinski, Stewart F. Parker, Ali Boudjada, Abdou Boucekkine

▶ **To cite this version:**

Soraya Zeroual, Jean Meinnel, Andrzej Lapinski, Stewart F. Parker, Ali Boudjada, et al.. Vibrational spectroscopy and DFT calculations of 1,3-dibromo-2,4,6-trimethylbenzene: Anharmonicity, coupling and methyl group tunneling. Vibrational Spectroscopy, 2013, 67, pp.27-43. 10.1016/j.vibspec.2013.03.007 . hal-00906659

HAL Id: hal-00906659
https://hal.science/hal-00906659

Submitted on 10 Dec 2013

HAL is a multi-disciplinary open access archive for the deposit and dissemination of scientific research documents, whether they are published or not. The documents may come from teaching and research institutions in France or abroad, or from public or private research centers.

L'archive ouverte pluridisciplinaire **HAL**, est destinée au dépôt et à la diffusion de documents scientifiques de niveau recherche, publiés ou non, émanant des établissements d'enseignement et de recherche français ou étrangers, des laboratoires publics ou privés.

Vibrational spectroscopy and DFT calculations 1, 3-dibromo-2,4,6-trimethylbenzene. (Anharmonicity, Coupling and Methyl group tunneling)

S. Zeroual[1, 2], J. Meinnel[2]*, A. Lapinski[3], S.Parker[4], A. Boudjada[1] and A. Boucekkine[2]

[1]*Laboratoire de Cristallographie, Université Mentouri, 25017, Constantine, Algérie*

[2] *Laboratoire Sciences Chimiques de Rennes, Université de Rennes 1,F-35042 Rennes Cedex, France*

[3]*Institute of Molecular Physics, Polish Academy of Sciences, Poznan, Poland*

[4] *Rutherford Appleton Laboratory, ISIS Facility, Didcot OX11,0QX, U.K.*

** Correspondence to: Jean Meinnel, Sciences Chimiques de Rennes, Université de Rennes 1,F-35042, Rennes, France*

E-mail: *jean.meinnel@cegetel.net*

Abstract- The Raman, IR and INS spectra of 1,3-dibromo-2,4,6-trimethylbenzene (DBMH) were recorded in the 80-3200 cm^{-1} range. The molecular conformation and vibrational spectra of DBMH were computed at the MPW1PW91/LANL2DZ level. Except for the methyl 2 environment, the agreement between the DFT calculations and the neutron diffraction structure is almost perfect (deviations < 0.01 Å for bond lengths, < 0.2° for angles). The frequencies of the internal modes of vibration were calculated with the harmonic and anharmonic approximations; the later method yields results that are in remarkable agreement with the spectroscopic data, resulting in a confident assignment of the vibrational bands. Thus, no scaling is necessary. The coupling, in phase or anti-phase, of the motions of symmetrical C-Br and C-Me bonds is highlighted. Our DFT calculations suggest that the torsion of methyl groups 4 and 6 is hindered in deep wells, whereas methyl group 2 is a quasi-free rotor. The failure of the calculations to determine the frequencies of the methyl torsional modes is explained as follows: DFT does not consider the methyl spins and assumes localization of the protons, whereas the methyl groups must be treated as quantum rotors.

Keywords: Raman spectroscopy; IR spectroscopy; Inelastic neutron scattering; DFT calculations; 1,3-dibromo-2,4,6-trimethylbenzene

1-Introduction

A tremendous amount of work has been devoted to the spectroscopy of polysubstituted benzenes. Among those relative to penta- and hexa-substituted compounds, two extensive papers were published in 1985: one paper compared eleven polymethyl-benzenes (pMeB) [1] and the second described six chloromethyl-benzenes $C_6(CH_3,Cl)_6$ (ClMeB) [2]. In these studies, the experimental spectra were assigned using normal coordinate calculations to determine a common multi-parameter force field. Because the molecular conformations were not accurately known the authors assumed that the aromatic ring in all molecules was a regular hexagon, that the bond angles were 120°, and the bond lengths were 1.396 Å for the carbon-carbon aromatic bond, 1.509 Å for the methyl carbon-aromatic carbon bond, 1.083 Å for the aromatic carbon-hydrogen bond and 1.096 Å for the methyl-carbon hydrogen bond. For the pMeB species, the Raman and infra-red measurements were performed with samples in the gaseous phase at approximately 550 K. A 46-parameter valence force field had been proposed, and the average error between the 736 observed and calculated wave-numbers was 6.4 cm^{-1}. This agreement suggests that the use of an excessive number of off-diagonal constants (interactions terms) allows us to compensate for the large errors done in the geometrical parameters. According to the authors in these previous studies: "there is a great stability of the internal methyl modes, in a limit of ± 5 cm^{-1} they are located at: 2930 cm^{-1} for the C-H stretching, 1445 cm^{-1} for the asymmetric C-H bending, 1380 cm^{-1} for the C-H symmetric bending, 1000 and 1060 cm^{-1} for the C-H rocking". For the "torsion mode" of the methyl groups, no experimental data were available. The authors assumed without proof that these groups are "free" rotors", which is rather rare for a methyl group in solid state molecules. On the contrary this finding is well established for one of the three methyl groups of dibromomesitylene that was studied in this paper.

The parent ClMB molecules were studied as crystals from room temperature to liquid nitrogen temperature. It was also assumed that in these molecules the benzene rings are perfect hexagons. Because the CH_3 group vibrations have been observed at similar frequencies to those in the pMeB molecules these groups were assumed to be not affected by the skeleton vibrations. Thus by considering the methyl group to be a point mass the authors were able to independently study the remaining 30 vibrations of the carbon-chlorine skeleton as those of a cyclic $C_6(X,Cl)_6$ system. Then, the authors used an optimized multi-parameter valence force field to reproduce the 121 assigned frequencies in seven different molecules. The potential energy was determined using nine principal force constants corresponding to nine different types of deformations (bond lengths and angles). To incorporate the interactions between the substituent vibrations and the deformations of the benzene ring, 37 near neighbor interaction coefficients were considered. In fact, using these

new interaction parameters partially corrects the errors introduced when using a regular hexagon for the benzene ring in these asymmetrically substituted molecules. Finally the calculated frequencies reproduce the observed frequencies with an average error of only 10.9 cm^{-1}.

In parallel to these empirical molecular mechanic calculations, quantum chemistry programs were established that were able to provide a molecular conformation in good agreement with the X-ray determination. In the late 1970s, the analytical second-derivative techniques were introduced at the Hartree-Fock (HF) level resulting in the sequence of the fundamental frequencies. However, when compared to the experimental frequencies, the computed HF frequencies were consistently 7-15 % too high. This overestimation of the frequencies may largely be attributed to the HF method itself because this method neglects electron correlation, basis set truncation and anharmonicity. Because the overestimation is fairly uniform, a proposed solution involves the application of a single scaling factor to the theoretical harmonic frequencies to provide better agreement with the experimental data. For example in 1981, Pople et al. [3] proposed a scaling factor of 0.89 for a set of 38 molecules (477 HF/3-21G harmonic frequencies). The need for this type of correction diminishes when using density functional methods because these methods include –more or less empirically– a significant part of the total electron correlation. In 1996, Scott and Radom [4] improved the global scaling technique in their scaled quantum mechanical force field (SQMFF) procedure. They have shown that all DFT calculations, in particular those using B3-PW91/6-31G(d) or B-LYP/6-311G(df,p), were much more successful than those based on HF or MP2. At the same time, Pulay et al. [5, 6] proposed an alternative approach to the SQMFF method that involves a direct scaling of the primitive valence force constants. In a study of 60 molecules (1500 vibrational frequencies), these authors obtained an average error of less than 8.5 cm^{-1} in the scaled frequencies. This result corresponds to an average percentage error smaller than 1 %. Notably when one hydrogen atom is implied, the scaling factors proposed for the stretching (C-H, N-H, O-H) and bending (X-C-H, X-O-H, X-X-H, H-N-H) vibrations are in the range of 0.87 - 0.95, whereas the scaling factor for C-Cl stretching is 1.04. The agreement between theory and experiment was further improved using larger basis sets in the DFT computations. Thus, the majority of Raman and IR experimental spectra are now assigned using DFT calculations. In addition to the data provided by these two spectroscopic techniques, inelastic neutron scattering (INS) furnishes new information because of the absence of selection rules and the predominance of scattering due to hydrogen atoms. An example of a study of symmetrical molecules is a paper describing sym-$C_6F_3H_3$ and C_6F_6 [7], in which the results of DFT calculations (using five different basis sets) were used to

assign the lines observed in Raman, IR and INS spectra. The INS spectrum of C_6F_6 directly exhibits seven bands of the nine vibrations that are inactive in the Raman and IR spectra. The overall RMS for the agreement between calculation and experiment is better than 20 cm^{-1}, demonstrating the high quality of the theoretical predictions.

Currently, each year, several new publications are presented describing studies of substituted benzenes using a combination of Raman and IR spectroscopies and DFT or HF theoretical calculations. Curiously, no systematic spectroscopic studies of mesitylene (or 1,3,5-trimethyl-benzene) derivatives have been undertaken whereas extensive studies of the protons tunneling in methyl groups have been published [8]. For the trichloro- tribromo- and triiodo-mesitylene (TCM, TBM, TIM) species, INS on powder samples [9] and on single crystals [10, 11] has been used to establish that the three methyl groups in each molecule have a different tunneling gap, which is contrary to what is expected for a molecule with true C_{3h} symmetry. For TIM, for example, three excitations were observed at 15, 24 and 89 μeV [8, 9]. This difference in tunneling gaps is due to the difference in the intermolecular interactions exerted on the methyl groups located in non equivalent sites in the triclinic crystal cell. Neutron diffraction studies of the molecular conformations have shown additional consequences: not only the proton probability density but also the orientation differs for each methyl group [12, 13,14]. These deviations from the ideal symmetry have visible consequences in the Raman and IR spectra at low temperatures (< 50 K): the inactive modes for C_{3h} symmetry become visible whereas the previously degenerate modes E' and E" are split [15]. The influence of intra and intermolecular symmetry on the tunneling properties of the methyl groups is still more spectacular in the case of the fully hydrogenated dibromomesitylene ($C_9Br_2H_{10}$ or DBMH) [16]. In this compound, the methyl group surrounded by two bromine atoms behaves as a quasi-free rotor, and its tunneling gap as using INS is large (387 μeV or 3.1 cm^{-1}). Furthermore, several torsional modes have been observed in the range 1.7 - 4 meV (14-32 cm^{-1}) using INS [16, 17] and also Raman diffusion [18]. In contrast, the rotation of the two other methyl groups located between one bromine atom and one hydrogen atom is highly hindered, and the tunneling gap is less than 1 μeV [17]. Therefore, we have undertaken a detailed study of the vibrational modes of DBMH with the intention to detect other spectroscopic consequences of the presence of two types of methyl groups.

2. **Molecular conformation of dibromomesitylene DBMH.**

The structure of DBMH has already been determined using neutron diffraction on a single crystal. Table 1 lists the values of the bond lengths and angles obtained using neutron diffraction at 120 and 14 K that have been published [19]. These values must be compared with the results of DFT calculations obtained under different symmetry conditions.

2.1. Molecular conformation of DBMH determined using neutron diffraction at 14 K and 120 K.

The thermal differential analysis indicated that DBMH exists in two different crystal phases with an order-disorder transition at 292 ± 0.3 K.. The structure of the low temperature ordered phase was solved by Hernandez et al. using neutron diffraction with a single crystal [19]. The crystal is monoclinic and assigned to the space group $P2_1/n$ with 4 molecules in the unit cell. The molecules form molecular columns parallel to the ***a*** axis. In these columns, the arrangement is 'anti-dipolar'. The structure determination was performed with a great accuracy, the goodness factor R being 0.032 at 120 K and 0.026 at 14 K. The experimental bond lengths and angles are listed in Table 1 and depicted in Fig. 1b.

Table 1

Figures 1a, 1b, 1c

The hexagonal ring in DBMH is distorted. There are large differences between the six intra-cyclicangles, these angles vary from 115.8° for C_1-C_2-C_3 to 123.6° for C_2-C_3-C_4. Thus, using a mean value of 120° as was used in [1, 2] should be a very crude hypothesis. Fig. 1b relative to the molecular conformation determined at 14 K suggests that the C_{2v} symmetry prediction is fulfilled to a good degree of accuracy. There is a plane of symmetry P_{perp} perpendicular to the benzene ring bisecting carbon atoms C_{m2}, C_2, C_5 and hydrogen atom H_5. The proton probability densities (PPD) relative to Me_4 and Me_6 are well localized with three peaks (Fig. 2), corresponding to three well localized protons. In contrast, the PPD in Me_2 is delocalized on a ring with six broad maxima from the refinement (Fig. 1b and 2) or from the map of a Fourier difference performed in the plane of the nuclei of the three hydrogen atoms of the methyl group (Fig. 2). The extra-cyclic angles $C_1C_2C_{m2}$ and $C_3C_2C_{m2}$ are equal to 122.0° in the limit of 0.1°, which is contrary to those observed for Me_4 and Me_6, for which the extra-cyclic angles are 120.2° on one side and 122.7° on the other side (Table 1 and Fig. 1b). The small departure from symmetry observed at 120 K between the angles $Br_1C_1C_2$ and $Br_3C_3C_2$ was not observed at 14 K. One important result is that if the thermal librational scattering

(TLS) is considered during the neutron diffraction (ND) refinement, the benzene ring is determined to be planar with an accuracy greater than 0.005 Å. Therefore, it can be concluded from the ND results that in the solid state, the DBMH molecule retains two planes of symmetry: the ring plane (P_{ring}) and one plane (P_{perp}) perpendicular to P_{ring}. The intersection between these two planes is the axis of symmetry $\mathcal{C}_2$.

Figure 2

2.2. DFT calculations of the molecular conformation

All of the computations were performed using the Gaussian 2009 program package [20]. The DFT calculation that yielded the equilibrium conformation is referred to as "Cal_1 P_{ring}" in Table 1 and Fig. 1a. This conformation was obtained using the MPW1PW91 functional with the LANL2DZ basis set augmented with polarization functions on all atoms except for the hydrogen atoms. At equilibrium the benzene ring is a plane of symmetry. There is a remarkable agreement between the calculated values and the experimental data for the molecular region containing Me_4, H_5 and Me_6 and good agreement for the angles around C_4, C_5 and C_6 with a tolerance of 0.1°. The calculated bond distances are slightly larger than the experimental distances by only 2 to $4x10^{-3}$ Å. Importantly, in the equilibrium conformation, the two methyl groups Me_4 and Me_6 have one CH bond located in the ring plane P_{ring} that points towards the atom H_5. This finding is in perfect agreement with the C_{2v} symmetry observed for the molecule using neutron diffraction. These orientations of Me_4 and Me_6 groups correspond to very stable orientations: the barrier hindering the rotation of these groups has been calculated to be 490 cm^{-1}. In contrast, the configuration calculated for the environment of the third methyl group, Me_2, is not consistent with the C_{2v} symmetry. At equilibrium, the calculated structure corresponds to a methyl group with three punctual protons and one CH bond in the plane of the aromatic ring. It is clear from Fig.1a that the left and right sides of the molecule around Me_2 are not symmetric; this lack of symmetry occurs because the trigonal symmetry of the methyl group is not compatible with the C_{2v} symmetry of its environment which consists of two equivalent pairs of carbon-bromine atoms C_1-Br_1 and C_3-Br_3. The DFT optimized geometry has only C_s symmetry, with the aromatic ring as the symmetry plane P_{ring}. It is possible to estimate the height of the barrier hindering the Me_2 "rotation" using this DFT computation. The calculated barrier of 53 cm^{-1} is ten times smaller than that of the two other methyl groups. This small value partially explains why the DFT computations could lead to the actual conformation of this group. The true source of discrepancy is the strict application of the Born-Oppenheimer approximation to protons and not

considering the spin of the methyl groups: proton spins are central to the phenomenon of "proton rotational tunneling" and thus to spatial delocalization [10] and to the existence of NMR. Another molecular conformation was obtained using the DFT computation "Cal_2 P_{perp}" involving the same functional and basis set, but constraining the plane P_{perp} containing C_{m2} and H_5 to be perpendicular to the initial ring plane P_{ring} as a symmetry plane (Fig.1c). In a normal projection onto P_{ring}, the "left" and "right" sides of the molecule are now symmetrical. The agreement between the experimental results and those obtained using Cal_2 is better than 0.005 Å for the bond lengths and better than 0.3° for all of the angles; therefore, Cal_2 provides a better representation of the molecular geometry than Cal_1 does for the environment around Me_2. To obtain this new orientation of Me_2, it is necessary to admit the loss of planarity of the aromatic ring; however, these deviations are very small: 8.10^{-3} Å for atom C_2, $15x10^{-3}$ Å for atom C_{m2} and $-3x10^{-3}$ Å for the Br atoms. The extra-cyclic angles around the C_2-C_{m2} bond are now equivalent and equal to 122.9°. But, a new problem has been introduced. There are now two possibilities for the displacement of the atom C_{m2} relative to the plane P_{ring}: i.e. above or below the plane? To summarize, the two calculations Cal_1 and Cal_2 provide molecular conformations that, with the exception of the Me_2 group, are not significantly different from the experimental geometry. The energy of formation found by Cal_2 is less favorable than that found by Cal_1 by only 200 cm^{-1}, it concerns almost exclusively Me_2 environment. This explains that only the modes implying mainly Me_2 could be altered by the choice of the equilibrium structure.

3. Spectroscopic measurements, experimental details

The commercially purchased DBMH (Sigma-Aldrich, F) was purified by crystallization using a solution in chloroform and pumping the solvent. This step was followed by a vacuum sublimation. Small single crystals were obtained by slowly crystallizing the purified compound from a solution of methanol.

3.1. Raman spectra: Table 2, Fig. 3a, 3b, 3c and 6b.

The Raman spectra of DBMH were measured using a Horiba Jobin-Yvon HR 800 Raman spectrometer. The excitation source was a He-Ne laser operating on the 632.817 nm line. The spectra were recorded at 288 K in the 80 - 4000 cm^{-1} region with a resolution of 3 cm^{-1}. It was possible to use single crystals with dimensions as small as 20x20x100 μm^3. Thus, we obtained two types of Raman polarized spectra. In the first orientation (Fig. 3b), the polarization vector $\mathfrak{E}$ of the incident

laser beam was approximately in the ***bc*** crystallographic plane, i.e., it was oriented at an angle smaller than 20° relative to the DBMH ring plane. In the second orientation (Fig. 3c), the electric field $\mathfrak{E}$ was oriented approximately along the crystallographic axis ***a***, i.e., it was oriented at an angle approximately 18° relative to a line perpendicular to the ring plane. Thus, in the case of similar Raman activities, the intensity of an in-plane vibration band is larger in the spectrum shown in Fig. 3b, while an out-of-plane vibration band is stronger in the spectrum shown in Fig. 3c. Table 2 lists the Raman band positions observed at 288 K (column 3) and the relative experimental intensities of these spectral features (column 16) in comparison with the calculated intensities (column 15). The spectrum recorded in the 2800 - 3200 cm^{-1} range is shown in Fig. 6b.

3. 2. Infra-red spectra at room temperature: Table 2, Fig. 4a, 4b & 6c.

The infra-red absorption spectra were measured from 400 to 4000 cm^{-1}, using a Fourier transform spectrograph (Bruker Equinox 55) and using the KBr pellet technique. The resolution was approximately 2.5 cm^{-1}. The IR range of 100 - 400 cm^{-1} was investigated using another Fourier transform spectrograph (IFS 125 MR) with synchrotron radiation on the AILES line at SOLEIL. The sample was a pellet of compressed pure DBMH that was 1mm thick. The resolution was better than 1 cm^{-1}. The frequencies of the IR absorption lines observed experimentally in the range (Fig. 4b) are given in Table 2, column 4. The calculated relative intensities of these features are listed in column 17, and those observed experimentally are in column 18. The spectrum recorded in the 2800 – 3200 cm^{-1} region is depicted in Fig.6c.

3. 3. Inelastic neutron scattering spectra

The INS spectra were obtained using the TOSCA-II inelastic spectrometer of the ISIS pulsed neutron source at Rutherford Appleton Laboratory (Chilton, Didcot, U.K.). TOSCA-II is a crystal-analyzer inverse-geometry spectrometer. The incident neutron beam spans a broad energy range that covers the energy transfer region from 4 to 500 meV (30 - 4000 cm^{-1}). The final energy of the scattered neutrons (approximately 3.35 meV) was selected by two sets of pyrolytic graphite crystals placed nearly at 43° and 138° relative to the incident beam. Because of this fixed geometry, the wave-vector transfer *Q* is roughly proportional to the square root of the incoming neutron energy. The energy resolution in the accessible energy range allows a resolution better than 3 cm^{-1} for *Q* smaller than 700 cm^{-1}. The samples were pellets approximately 1 mm thick, resulting in a surface area of 3x4 cm^2,

packed in an aluminum pocket. Approximately 2 g of DBMH was used, and the samples were frozen below 30 K in an "orange" helium cryostat. The frequencies of the maxima of the scattered neutrons are given in Table 2, column 5, and illustrated by Fig.5.

4. Calculations of the frequencies of the normal modes of vibration

4.1. Comparison of "harmonic", "harmonic scaled" and "anharmonic" frequencies calculated by DFT, the ring plane P_{ring} being a plane of symmetry

Table 2 lists the results of three DFT calculations of the normal modes of vibration that were performed using the Gaussian 2010 [20] program package. These results were obtained using the MPW1PW91 functional with the LANL2DZ basis set augmented with polarization functions. The equilibrium molecular geometry is that presented in section 2.2, the ring plane P_{ring} being a plane of symmetry. The DBMH molecule containing 21 atoms has 57 optical modes of vibration. Relatively to the plane of symmetry, the 57 modes of vibration may be divided into two types: 36 are of symmetry A' (in-plane), and 21 are of symmetry A" (out-of-plane) (see column 2, Table 2). The calculated modes are numbered from the largest frequency to the smallest within each fundamental frequency. The frequencies may be compared with the experimental results from the Raman spectroscopy at 288 K (column 3) or, if the Raman intensities are too small, to the IR data (column 4) or to the INS data (column 5). The ω_h wave numbers (column 10) correspond to the frequencies that were calculated by assuming the harmonic approximation without any scaling. These ω_h frequencies are larger than the experimental frequencies by 14 to 72 cm^{-1} in the range of 600 - 1700 cm^{-1} (i.e. 2 to 4 %), by 160 to 230 cm^{-1} in the range of 2800 – 3250 cm^{-1} (i.e. 6 to 8 %), while between 150 and 600 cm^{-1} there are fluctuations amounting to ± 3 %. The five smallest calculated frequencies should be treated separately because they must contain the three methyl groups "torsions" and are very sensitive to the type of calculation. These DFT computations also predict the quantitative specificities of the IR and Raman lines. In fact, the Gaussian program calculates the Raman activity S_i for each normal mode n° i of an isolated molecule. We calculated the Raman activity in parallel to the ω_h frequencies assuming the harmonic approximation (see column 14 Table 2). The result was then converted to Raman intensity using the following relationship derived from the intensity theory of Raman scattering [21, 22, 23]

$$I_i = C\,(\omega_0 - \omega_i)^4\, S_i \,/\, \omega_i\, [1 - \exp(-h\,c\,\omega_{Ri} / kT)]$$

where ω_0 is the laser excitation frequency in cm^{-1} (in our experiments ω_0 = 15802 cm^{-1}) ω_i is the vibrational frequency of the i-th normal mode in cm^{-1}, h and k are the Planck and Boltzmann

constants, T is the temperature in Kelvin and C is a suitably constant chosen that serves as a common normalization factor for all peak intensities. For these spectra, we chose a relative intensity of 100 for excitation n° 41 calculated at ω_h= 560 cm^{-1} and observed at ω_i = 563 cm^{-1}, because it is for this band that the intensity calculated in the range 200-1600 cm^{-1} is the highest. The relative intensities calculated for the Raman spectra are found in Table 2, column 15, and are represented in Fig. 3a. These intensities must be compared to those observed in the spectra: (column 16). However, because the Raman spectra were obtained with oriented crystals, it is possible to independently estimate those intensities arising from "in-plane" vibrations (Fig. 3b) and those arising from vibrations perpendicular to the molecular plane (Fig. 3c). Nevertheless, this estimation must be performed with caution because the spectra were obtained near room temperature, which means that the lines are broadened and only peak maximum intensities may be estimated.

To obtain a better agreement between theory and experiment, it is customary to scale down the calculated harmonic frequencies [4, 5, 6]. Recently, empirical scaling factors have been proposed after DFT calculations on benzenic compounds: 0.957 for tolunitrile [24], 0.960 for p-chlorobenzoic acid [25] and 0.958 and 0.983 for halogenoanilines above and below 1700 cm^{-1}, respectively [26, 27, 28]. Column 9b lists the values of the ratio ω_R / ω_h between our Raman experimental and calculated values. These values vary from 0.935 to 1.013. As a result, we multiplied frequencies ω_h by the "often used" scaling factors of 0.958 for frequencies larger than 1800 cm^{-1} and 0.983 for the other frequencies, thus obtaining the ω_{hsc} frequencies listed in column 8. The new differences between theory and experiment (ω_{hsc} - ω_R) (column 9) are smaller than the preceding differences (ω_h - ω_R) by a factor 2 to 3 for frequencies larger than 700 cm^{-1}. Only the frequencies calculated for the C-H stretching vibrations remain too large, by 40 to 95 cm^{-1}, and could be better estimated using a scaling factor of approximately 0.94. It is essential to determine whether the discrepancies between theory and experiment are mainly due to the neglect of the anharmonicity of the potential energy in the calculations. Thus, we computed the "anharmonic frequencies" (ω_{anh}) using the automated code implemented in Gaussian by Barone [29]. Starting from the optimized geometry, the program computes the third and semi-diagonal fourth derivatives of the formation energy and then evaluates the ω_{anh} frequencies of the fundamental bands using second order perturbation theory (keyword: *freq(anharmonic)*). This calculation also provides the frequencies of the overtones (ω^o_{anh}) and those of the combination bands (ω^c_{anh}). The ω_{anh} frequencies of DBMH are listed in column 6 of Table 2, and the deviations from the experimental values, ω_{anh} - ω_R are given in column 7. It appears that the agreement is remarkable in the entire range of 130 -1500 cm^{-1}, this agreement is even better than that

observed for the scaled frequencies; the deviations are smaller than 15 cm^{-1} for 39 of the 41 modes. The agreement is also greatly improved for the C-H stretching modes (ω_{anh}) and is now overestimated by less than 3% (compared to the previous 8%) for the "harmonic" frequencies ω_h. These results for DBMH, a poly-methylated molecule, confirm the ability of the analytical second-order perturbation treatment to consider the anharmonicity during the calculation of the internal modes of vibration. Similar results have also been observed in studies of azabenzenes [29, 30, 31], pyrrole and furan [32], uracil [33] or, more recently, monofluoroanilines [26]. The anharmonic frequencies ω_{anh} obtained for DBMH are in very good agreement with the experimental values, and this agreement is even better than that observed for ω_{hsc}, whose values were obtained semi-empirically using the scaled quantum mechanical method. Thus, for the assignment of each type of motion to a specific frequency, we will only compare ω_R (or ω_{IR}) and ω_{anh}.

4.2. Calculations of the frequencies of the normal modes of vibration assuming that the plane of symmetry is the plane P_{perp} perpendicular to the benzene ring: Table 2 columns 12-13

In the case of DBMH, it must be remembered that the model used in the DFT calculations does not perfectly represent the environment of the methyl group Me_2. Section 2.2 discussed another calculation that was performed when the molecule is constrained to have a symmetry plane P_{perp} normal to the ring plane. This conformation is illustrated in Fig. 1c and takes into account the symmetry around the Br_1 and Br_2 atoms and the Me_2 substituent. It corresponds approximately to the neutron diffraction structure although it partially breaks the planarity of the benzene ring. However, for DFT calculations, this conformation corresponds to an unstable equilibrium in energy and is located on a saddle point. It is of interest to determine whether this conformation still provides valuable vibrational frequencies. Consequently, a fourth set of data was calculated using the harmonic approximation which is presented as ω_{hp} in column 12. The vibrations of the new symmetries A' and A" correspond to symmetrical (Sym) and antisymmetrical (AntiSym) motions, respectively for the bonds that are equivalent by symmetry such as C_1-Br_1 and C_3-Br_3 for example . The calculated frequencies are listed in Table 2, column 12. All of the differences (ω_h - ω_{hp}) are smaller than 4 cm^{-1} (column 13), with the exception of the lowest frequencies that are in direct connection with the Me_2 torsion. Thus, the majority of the overestimation of the unscaled harmonic frequencies is effectively caused by the anharmonicity of the atomic motions, particularly those of the hydrogen atoms. The two geometric models, that are slightly "imperfect" relatively to the neutron

scattering structure, are practically equivalent for the DFT calculations, except for mode n° 57, which is relative to the torsion of the Me_2 group (see below).

Table 2

4.3. A distinction between the internal vibration modes and the lattice modes

For a DBMH crystal below 292 K, there are four molecules in the monoclinic $P2_12_12_1$ cell, thus, 6 Z "Iattice modes" are predicted, where Z is the number of molecules in the unit cell. Consequently, 21 new optical modes are expected. Generally, the intensity of the lattice modes in the Raman spectra is smaller than that of the internal modes. In a previous study conducted at approximately 4 K [18], almost all of these lattice modes occured at frequencies smaller than 100 cm^{-1}. The widths of the bands grew quickly as the temperature increases, so that the peaks are very flat at 288 K and difficult to detect. In Fig. 5, five peaks with maximum scattering of neutrons are detected below 135 cm^{-1} at a temperature of approximately 10 K. In these experiments, the scattering due to hydrogen atoms is the most intense phenomenon. This region has been studied in previous experiments examining the proton tunneling of the methyl groups [16, 17]. Thus, if peaks at 61, 79, 91 cm^{-1} originate in transitions 1^A-2^A, O^E-2^E and O^A-2A between torsional levels of Me_2, only the peaks at 117 (124 in R), 135 and 156 (157 in R) may be assigned to internal modes.

5.Vibrational spectra and their assignments

5.1. Labelling of the internal coordinates used to describe the vibrations.

The labeling used to describe the vibrations is that proposed by Decius and alt. [34]. When the atomic displacements occur in the symmetry plane (i.p.), the variations in the lengths or angles (Fig. 1b) are labeled as follows: t_n = stretching of a C_n-C_{n+1} bond into the ring (n=1-6), s_p = stretching of a C_p-C_{mp} bond for a methyl substituent n° p (p = 2, 4, 6), s_i = stretching of a C_i-Br_i bond for a bromine substituent n° i (i = 1 or 3), s_5 = stretching of the C_5-H_5 bond, α_n = C_{n-1}-C_n-C_{n+1} ring angle breathing, and β_n = in-plane bending of a C_n-X_n bond, knowing that ϕ_{nd} = X_n-C_n-C_{n+1} and ϕ_{ng}= C_{n-1}-C_n-X_n are outer ring angles, and in consequence β_n= ϕ_{nd} - ϕ_{ng} and α_n = 360° - (ϕ_{nd} + ϕ_{ng}). A positive ϕ_n = ϕ_{nd} + ϕ_{ng} angle corresponds to a clockwise motion. The following labels apply for a motion within a methyl group n° p: r_{pa} = stretching of the C_{mp}-H_{pa} bond (in the ring plane), r_{pb} and r_{pc} correspond to the two staggered C-H bonds, and η_p = 'i.p." torsion of the axis of this methyl group Me_p. For example, η_4 corresponds to symmetrical rotations of planes C_4-$C_{m4}H_{4b}$ and C_4-C_{m4}-H_{4c} around the

C_4-C_{m4} bond relative to the ring plane. χ_{pa} denotes the C_p-C_{mp}-H_{pa} variation with $\chi_p = \chi_{pa} + \chi_{pb} + \chi_{pc.}$ whereas θ_{pa} denotes the H_{pb}-C_{mp}-H_{pc} angle variation with $\theta_p = \theta_{pa} + \theta_{pb} + \theta_{pc}$.

The out-of-plane (o.p.) motions are labeled as follows: γ_n = out-of-plane bending of a C_n-X_n bond, it is also named wagging [2], τ_i = out of-plane benzene ring torsion of a C_i-C_{i+1} bond and δ_p = sum of out-of-plane torsion of the methyl C-H bonds around the C_p-C_{mp} bond. For deformations inside the methyl groups, $r''_{mp} = C_{mp}$-H_{pi} for the o-p methyl group stretching (i = a, b or c) when the atom C_{mp} and H_{pi} move out of the ring plane P_{ring}, χ''_p = sum of angles for the C_p-H_{pi}-H_{pi+1} variations, θ''_p = sum of angles for the variations C_p-C_{mp}-H_i. Two remarks must be added. First, if during a large wagging γ_n the substituent X_n moves up then the carbon C_n is moving down relative to the atoms C_{n-1} and C_{n+1} in the ring, this generates small ring torsions τ_{i-1} and τ_i; secondly, for a ring torsion τ_i there is also a displacement of the bond C_i-X_i in the same direction than C_i, this will be noted κ_i and is distinct from a γ_i for the PED calculations.

5.2. Calculation of the potential energy distribution (PED) for each mode.

To understand the molecular dynamics, it is useful to visualize the individual deformations of the bonds and angles. A first approach was obtained based on the information presented in Fig. 7, 8 and 9. These figures were drawn using the Molekel 98 package to visualize the deformations that are characteristics of each frequency ω_h. This qualitative approach was completed using a quantitative estimation of the potential energy distribution, the PED. The PED was obtained using the key-word *freq(internal)* in the Gaussian package. Table 3 provides the contribution to the PED for each mode due to the principal in-plane deformations. Table 4 lists the PED for the out-of-plane deformations. The two approaches are not strictly equivalent because a large displacement of a light hydrogen atom has a smaller relative contribution to the PED than a displacement of a Br atom or a Me group does. These tables list the main deformations, for equivalent atoms, the + sign indicates motions in-phase, and the – sign indicates opposite motions. The numbers indicate the percentage of each contribution to the PED.

Table 3

5.3. A criterion for validity: the calculation-experiment agreement for the most intense frequencies:

A first test to confirm the ability of the DFT calculations to accurately predict the experimental data is to examine the sequence of the intense lines in the IR and Raman spectra that are presented in Table 2 (columns 15-18) and in Figs. 3 and 4. The criterion for the comparison requires the relative

intensity to be larger than 50 for the experiment and greater than 30 for the calculations (reference 100 for band n° 41 observed at 560 cm^{-1} in the Raman spectra). The experimental and calculated frequencies will be compared and indicated in the following order: in first the frequency observed, ω_R, and then, inside parentheses, (ω_{anh}) the "anharmonic" frequency calculated using DFT. The intense bands observed in the Raman spectra are located at: 157 (153), 252 (248), 561 (560), 590 (586), 1306 (1313), 1387 (1392) and 2923 (2977) cm^{-1}. The intense bands in the I.R. spectra are observed at:190 (166), 228 (222), 253 (248), 296 (288), 636 (637), 852 (854), 960 (962), 1043 (1041), 1375 (1378), 1456 (1460) and 2920 (2977) cm^{-1}. The inelastic neutron scattering spectrum (Fig. 5) confirms the presence of essentially all of the modes calculated below 1000 cm^{-1}, particularly several weak peaks that were difficult to detect in the IR or Raman spectra. For example, column 5 of Table 2, one may note the high intensity for the scattered lines at 193, 365, 542, 853 and 1031 cm^{-1}. The agreement between the calculated and observed frequencies is remarkable. The success of the first inspection encouraged us to pursue a detailed assignment of the bands observed experimentally.

5.4 Regarding the labels: in-plane or out-of-plane mode, "methyl" or "skeleton" vibrations, symmetric or anti-symmetric modes

Because there are 21 atoms in the DBMH molecule, 57 normal modes of vibration are expected. In our calculations the plane P_{ring} is a plane of symmetry for the equilibrium conformation. Thus, there are 36 vibration frequencies with symmetry A' for which the motions of the Br, C, and H_a atoms occur within the plane P_{ring}. These vibrations are illustrated in Figs. 7 and 8. For the 21 other vibrations which have symmetry A", these atoms are moving normally to P_{ring} as shown in Fig. 9. Of the 57 modes of vibration, 27 modes must correspond to the stretching of the C_m-H bonds (r_{mp}, $r"_{mp}$) or to deformations of the C_{ring}-C_{methyl}-H_i entities (, δ_{pp}, χ_p, θ_p, $\chi"_p$, $\theta"_p$). These modes will be entitled "methyl modes of vibrations". The criterion to validate this label is that the contribution of the methyl deformations to the PED is larger than 60 %. As mentioned in the introduction section, the methyl groups linked to an aromatic ring are characterized by specific modes concentrated in narrow bands, appearing around 3000 cm^{-1}, 1445 cm^{-1}, 1380 cm^{-1}, 1060 cm^{-1} and 1000 cm^{-1} and below 150 cm^{-1}. The 30 other modes must therefore mainly involve the aromatic ring and its substituents and may be labeled as "skeleton vibrations". These vibrations are located throughout the region below 1700 cm^{-1}. A rapid examination of Table 2 shows that 24 frequencies are smaller than 1000 cm^{-1} and may correspond to 21 skeleton modes and the three methyl torsion modes. Thus, only 9 "skeleton modes" are expected in the range of 1000 – 1700 cm^{-1}. The pictures in Fig. 7 reveal the importance

of the pseudo-symmetry relative to P_{perp} perpendicular to P_{ring}. DFT calculations done with the conformation of Fig. 1c are given Table 2, column 12b. If the atoms that are located symmetrically relative to this plane have in-phase displacements, the vibrations are of symmetry species A', if they are moving in opposite directions they have the symmetry species A". In the text, we will refer to vibrations as Sym or Antisym, respectively.

5.5. Assignment of specific in-plane vibrations to normal modes of species A'.

To describe the spectral assignments, the characteristic number of the vibration in order of decreasing observed frequency is given in first, it is followed by the experimental frequency ω_R (or ω_{IR}) and by the calculated frequency ω_{anh} written within parentheses The Sym "skeleton modes" of species A' correspond to the eleven pictures in the upper part of Fig. 7, whereas the ten Antisym modes are shown in the lower part of the figure. The "methyl modes" are represented in Fig. 8.

5.5.1. In plane skeleton modes implying large radial displacements (Tables 2 and 3, Figs. 7)

Mode n° 49, ω_R = 253 (248) cm^-1, involves Sym stretches of the C_1-Br_1 and C_3-Br_3 bonds (22%) with a Sym variation of the opposite α angles (9%) it is associated with Sym bendings of C_4-C_{m4} andC_6-C_{m6} (β_4-β_6) (20%) All of these motions are in perfect agreement with the presence of a mirror of symmetry, which is the plane P_{perp}. Mode n° 47, ω_{IR} = 295 (288) cm^{-1}, consists in AntiSym motions of the same atoms: stretches (18%) and bending (15%), of C-Br bonds which are associated with AntiSym breathing vibrations involving angles $-\alpha_4+\alpha_6$ opposite to methyl groups 4 and 6) (24%). These two modes, n^{os} 49 and 47, illustrate the splitting of the "C-Br stretching vibration" as a result of a coupling between the motions of the C_1-Br_1 and C_3-Br_3 bonds. The Sym mode n° 41 , ω_R = 561 (560) cm^{-1}, is mainly due to ring breathing: two Sym angles enlargements ($\alpha_1+\alpha_3$) (20%), two angle reductions ($-\alpha_2-\alpha_5$) (28%). Mode n° 40, ω_R = 590 (586) cm^{-1}, is also a Sym mode, it is mainly due to Sym C-C_m stretching vibrations (14%) plus reduction of the corresponding angles ($\alpha_4+\alpha_5+\alpha_6$) (44%), Mode n° 38, ω_{IR} = 636 (637) cm^{-1}, has contributions similar to those of n° 40 but arranged in an AntiSym manner. Sym mode n° 35, ω_R = 940 (947) cm^{-1}, involves: Sym stretching vibrations of the C-C_m bonds (11%), cycle angles variations (15%) and Sym. tilting vibrations (52%) of the Me_4 and Me_6 groups. These deformations are similar in nature and intensity to the "methyl" rocking vibrations indicating strong interactions between the ring and methyl group motions in this frequency range. For AntiSym mode n° 34, ω_{IR} = 962 (960) cm^{-1},

almost one half of the contributions are attributed to AntiSym pairs of C-Br and C-C_m stretching vibrations: (16%) and the corresponding angles variations (21%), and the other half is a result of the Me_2 tilting vibration (34%). Note that for these two modes, $n°^s$ 34 and 35, the methyl groups have a contribution to the PED as large as that of the "skeleton" motions. The Sym mode n° 27, ω_{IR} = 1047 (1043) cm^{-1}, can be described as the trigonal ring-breathing mode or the 'star of David' vibration, it implies dilatations of three ring angles (25%) accompanied by contractions of the three others (23%). Sym mode n° 24 , ω_R = 1305 (1314+1322) cm^{-1}, is also a trigonal breathing mode consisting of stretching motions of the three C_p-C_{mp} bonds (15%) associated with alternate ring angles breathing (12%) while methyl umbrella deformations contribute 39%. Sym mode n° 20, ω_R = 1387 (1392) cm^{-1}, is due to Sym stretching motion C_p-C_{mp} bonds (13%)but again contributions from the umbrella bending motions of Me_2 and Me_6 (65%) are larger than those of the skeleton indicating strong interactions in this frequency region. For Sym mode n° 1, ω_{IR} 3014 cm^{-1} (3085), almost all the PED is due to stretching of the C_5H_5 bond.

5.5.2. In plane skeleton modes implying large tangential displacements (Tables 2 and 3, Figs. 7)
Among the remaining i.p. skeleton modes only four have relative intensities in the calculated Raman spectra that are larger than 20%: n^{os} 53, 46, 11 and 12, which is in agreement with the experimental results. N° 53 **,** ω_R = 157 cm^{-1} (153), primarily consists of the Sym scissoring motion of the two C-Br bonds (52%) with a slight stretching contribution(14%). **N**° 50, ω_R = (229 cm^{-1}(222), also involves the two C_i-Br_i bonds**,** but the bending motion in this mode is AntiSym (33%) with a small stretching character ($s_1 - s_3$) (17%). N° 46 is observed at 323 cm^{-1}(315), it involves the Sym bending (36%) of the pair C_4-Me_4 and C_6-Me_6 plus a Me_4 and Me_6 tilting motion (23%) N° 44 is observed at 374 cm^{-1} (360), this mode consists of the AntiSym bending motion of the C-C_m bonds (32%) and in-plane tilting motions of Me groups (24%) . Mode n° 42 is observed 541 cm^{-1}(542), it is an AntiSym bending motion involving an in-phase oscillation of the C-Br and C-C_m bonds ($\Sigma^n\beta_n$ ~ 50%) accompanied by in-plane tilting of the methyl group (34%). The AntiSym bending mode n° 26 (1217 cm^{-1}(1235) includes contributions from the bending vibration of the C_5-H_5 bond (28%)and tilting of the three methyl groups (34%).The mode n° 25, , ω_R = 1306 cm^{-1}(1314) ,corresponds to a trigonal deformation of the benzene ring caused by C_a-C_a stretching motions (33%) and large tilting motions of the methyl groups (42%). This mode is also referred to as the Kekule mode. The Sym stretching mode n° 21 may be a part of the broad band observed at 1387 cm^{-1}., this "skeleton" mode has very significant contributions from methyl groups. The AntiSym mode n° 19, ω_R = 1392 (1397) cm^{-1}, may

correspond to the peak in the IR spectrum at 1392 cm^{-1}. It consists of C-Br and C-C_m and C_5-H_5 motions (30%), and to a larger extent, umbrella deformations of the methyl groups (52%). Mode n° 12, ω_R = 1562 cm^{-1}(1588), corresponds to deformations of the C-C bonds in the benzene ring (32%), the vibrations are roughly parallel to the direction of the $\mathcal{C}_2$ axis. These vibrations are accompanied by a large narrowing of the α_2 and α_5 angles (15%) and enlargements of the $(\alpha_1+\alpha_3+\alpha_4+\alpha_6)$ angles (15%). AntiSym mode n° 11 has been detected at 1587 cm^{-1} (1629) with I_R = 15 (28). The deformations in the ring are perpendicular to P_{perp} and the α_2 and α_5 angles remain constant. All of these excitations are also detected in the INS spectrum (Fig. 5).

5.5.3. Assignment of the in-plane "methyl groups" modes of vibration

We previously proposed that the criteria for this labeling requires small contributions from the s, t, α,ϕ and/or β deformations but large contributions from the H-C-H (θ) and C-C-H (χ) bonds motions (> 30%) and from in-plane torsions (η) of the C-C_m bonds, i.e., more than 60% contribution to the PED from the methyl groups. In our experiments at 288 K, we observed a broadening of the lines so that the resolution was generally not sufficient to assign individual frequencies for Me_4 and Me_6 and individual intensities into these broad lines.

The calculated rocking modes of CH_3 are: N° 33 , ω_{IR} = 1013 cm^{-1} , n° 32, ω_R = 1028 cm^{-1} , n° 29 ω_R = 1024 cm^{-1}. The contribution of η_{pp} torsions to the total PED is almost equal to that of internal methyl deformations (χ,θ). Small bands are observed at 1015 and 1032 cm^{-1} in the Raman spectra (Fig.3) but it would be necessary to obtain spectra at much lower temperatures to propose a secure detailed assignment.

In-plane bending modes (or umbrella modes): For mode n° 23, ω_R = 1380 cm^{-1} (1378), the deformations of the Me_4 and Me_6 groups are in phase but out of phase relative to those of Me_2, For n° 22, ω_R = 1387cm^{-1} (1384), the deformations of Me_4 and Me_6 are in phase while Me_2 is at rest. For mode n° 20, ω_{IR} = 1387 cm^{-1} (1393), the deformations of Me_2 and Me_6 are in phase and out of phase to the small deformations of Me_4. The total intensity for these modes is distributed into a broad Raman band at 1387 cm^{-1} and must be associated with modes $n°^s$ 19 and 20.

In-plane bending (or scissor) modes of CH_3: In the IR spectra the sum of the relative intensities for n° 16 and that of the neighboring out-of-plane modes n^{os} 17-18 is I_{IR} = 45 in agreement with 30 calculated. For mode n° 16, ω_R = 1435 cm^{-1} (1438), the torsions η_2, η_4 and η_6 are calculated in phase while only the clippings for Me2 and Me6 are in phase. For mode n° 14, ω_R = 1456 cm^{-1}

(1462), the main contributions to the PED is calculated for Me_4. For n° 13, ω_R = 1456 cm^{-1} (1460), Me_4 is almost at rest, while Me_2 and Me_6 are moving in opposition.

Symmetric in-plane stretching (or breathing) modes of CH_3: N^{os} 10, 9 and 8 correspond to the broad and intense Raman line at ω_R = 2923 cm^{-1} (2977). For n° 10, groups Me_4 (48%) and Me_6 (42%) exhibit breathing motions that are out-of-phase (o.p.) For n° 9, these vibrations are in-phase (i.p.), and for n° 8, only Me_2 vibrates (88%).

Asymmetric in-plane stretching modes of CH_3: For these modes, in each methyl group the in-plane bonds C_{pm}-H_{pa} move in opposite direction to the staggered C_{pm}-H_{pb} and C_{pm}-H_{pc} bonds. Modes n^{os} 3 and 4 correspond to ω_R ~ 2978 cm^{-1} (3041) with I_R = 12 (36). **N° 2** corresponds to motions only within Me_2. This mode was calculated to be at 3066 cm^{-1} with a weak intensity, experimentally it appears as a bump in the IR spectra at 2985 cm^{-1}.

5.6. Out of plane modes (Tables 2 and 3, Figs. 3, 4 and 5)

In a Raman spectrum from a powdered sample of DBMH, it is more difficult to assign the o.p. modes than it is to assign the i.p. modes because the former have weaker intensities. Thus, we collected the Raman spectra shown in Fig. 3c using a small single crystal excited by a laser beam that was polarized approximately along the *b* axis of the crystal. Consequently, in this spectrum, the intensities of the i.p. vibrations are reduced and those of the o.p. modes are relatively enhanced which helps with the assignment. Nine normal modes of vibration of species A" were calculated and observed in the range of 1000-3050 cm^{-1}. For each of them the contribution of the CH_3 groups to the PED is larger than 60%, so they are labelled "methyl o-p modes". They are represented in the lower part of Fig. 9. Six A" modes located in the range of 200-1000 cm^{-1} were assigned as skeleton modes. For the six remaining modes, the torsion (hindered rotation) of the methyl groups plays a major part.

5.6.1. "Methyl groups" o. p. modes with frequencies higher than 1000 cm^{-1}

Table 4**. Fig. 6 and 9**

At 288 K, a broad band is observed at ω_R = 2956 cm^{-1} in the Raman spectra and at 2954 cm^{-1} in the IR spectrum. This band is located between two packets of i.p. modes already assigned: $n°^s$ 3 and 4 observed at ω_R = 2978 cm^{-1} (3041) and n^{os} 8, 9,10observed at 2923 cm^{-1}(2977). Thus, this band may be assigned to modes $n°^s$ 5, 6 and 7 calculated at ω_{anh} = 3015 cm^{-1}. For each mode, the internal motions involve stretchings of the two staggered C_m-H_{mb} and C_m-H_{mc} bonds, into a specific Me

group. The modes n°^{s} 15, 17 and 18 at ω_R = 1435 cm^{-1} (1440) are caused by the o.p. tilting motion δ and a type of clipping (χ",θ") within the methyl groups in almost equal proportions. The mode n° 15 involves only Me_2 (δ_2 = 47%). Mode n° 18 implies out-of-phase vibrations of Me_4 and Me_6 (δ_4 + δ_6 = 48%) whereas those vibrations are in-phase for mode n° 17 (δ_4 + δ_6 = 49%). Modes n^{os} 28 and 30 (ω_R = 1045 cm^{-1} (1035) are characteristic of the o.p. rocking motions of the methyl groups. Mode n° 28 concerns in phase o.p. vibrations involving Me_4 and Me_6. The vibrations are out-of-phase for mode n° 30 whereas for mode n° 31, ω_R = 1032 cm^{-1} (1028) only Me_2 is excited.

5.6.2. "Skeleton out-of-plane" modes

Table 4 gives a detailed panorama of the motions for each mode which are shown in the upper part of Fig. 8. These motions are complex and then difficult to describe in detail. Thus, we will indicate only the main contributions to the PED. For example, Sym mode n° 36, ω_{IR} = 853 cm^{-1} (854), is composed almost entirely of the o-p bending γ_5 (55%) of the C_5H_5 bond. Sym mode n° 37 seen by neutrons at ω_n = 698 cm^{-1} (708) is the trigonal puckering of the ring it consists mainly of alternate torsions τ_i up and down of the C-C in the ring (31%). AntiSym mode n° 39, ω_R = 588 cm^{-1} (583), consists of 20% of ring torsions, 21% of o.p. bending motions and 38% of methyl groups torsions. No° 43, ω_R = 517 cm^{-1} (526), appears as a Sym butterfly flapping around the $\mathcal{C}_2$ axis, it consists of 16 % of ring torsions, 36% of o.p. bending motions. No° 45, ω_R = 339 cm^{-1} (332), appears as an AntiSym motion. The PED contains 16% of ring torsion, 33% of o.p. bending motions and 36% of torsions of the methyl groups around their axes. No° 48, ω_R = 276 cm^{-1} (269), involves nearly the same motion as n° 45, but the ring oscillates now around an axis perpendicular to the $\mathcal{C}_2$ axis.

5.6.3. Methyl torsion modes and/or o.p. bending modes?

Mode n°51 (ω_{IR} = 190 cm^{-1}, ω_{anh} =166, ω_h = 188) is a type of breathing motion in which all atomic substituents move in the opposite direction of that of the ring carbon atoms, ($\Sigma\gamma_i$ = 19%). This mode results in an intense neutron scattering at 193 cm^{-1} and a medium I.R. absorption at 190 cm^{-1}, but it is inactive in Raman spectroscopy. Interestingly, there is also an important contribution to the PED (56%) due to torsions around the axis of the Me_4 and Me_6 groups. These torsion phenomena occur for all the modes with frequencies smaller than 200 cm^{-1}. For mode n°52, ω_R = 124 cm^{-1} (135), the calculations indicate in-phase librations of Me_4 and Me_6 groups, the largest contribution to the PED coming from Me_6 (57%). For mode n°54, ω_R = 124 cm^{-1} (136), the librations of the Me_2 and Me_6 groups are out of phase and the largest contribution to the PED is coming from Me_4 (63%). The

assignment of a Raman frequency ω_R for n°55 is difficult because its frequency cannot be known using the anharmonic approach (ω_{anh} = -145). Using the harmonic approximation, this mode was assigned as a Me_2 libration (δ_2 = 82%). Mode n° 56, ω_R = 88 cm^{-1} (66), corresponds to AntiSym C-Br bending ($-\gamma_1 + \gamma_3$) (26%) associated with a libration of Me_2 (23%). The anharmonic DFT calculations did not result in a real frequency for mode n° 57 (ω_{anh} = - 56). Using the harmonic approximation (ω_h = 71), the contributions to the PED are attributed to Sym C-Br bending vibrations ($\gamma_1 + \gamma_3$) (16 %) with a larger contribution from the torsional motion of the Me_2 group (53 %). These results confirm the particular behavior of the "symmetrical" methyl group Me_2. So it is now necessary to discuss the validity of these conclusions knowing the inadequacy of the DFT models to represent the molecular geometry around Me_2.

5.6.4. Remarks about the methyl groups torsion modes.

In section 2.1, we summarized the results of the structural studies involving neutron diffraction at 120 and 14 K. For the methyl groups Me_4 and Me_6, a "normal" conformation with three well defined maxima was observed with the protons probability density (PPD) [17]. In contrast, for Me_2, the PPD is widely spread over a torus. For Me_4 and Me_6, the DFT calculations generated an equilibrium conformation that is in agreement with the experimental results: for each methyl group, there is a preferred orientation with one C-H bond pointing towards the hydrogen H_5 (Table 1, Fig. 1a and 1c). Starting from these configurations, DFT calculations then provided values equal to 158 and 167 cm^{-1} using the harmonic approximation and equal to 135 and 136 cm^{-1} using the anharmonic approximation for the torsion mode of these groups. The calculated frequency does not vary significantly with the plane of symmetry (P_{ring} or P_{perp}) retained for the model molecule studied (Table 3). The intensity calculated for these excitations is very low in I.R., INS and Raman. In fact, based on inelastic neutron scattering experiment using a reduced fixed window [17], it was possible to estimate the hindering potentials V_3 of these methyl groups to be approximately 590 cm^{-1} plus a small out of phase component V_6 = 90 cm^{-1}. Using this potential, the "libration" transition 0^A-1^A (almost equal to 0^E-1^E) is approximately 145 cm^{-1}; this value is compatible with the preceding predictions relative to the Raman line at 136 cm^{-1}. The problem is different for the Me_2 group. A high-resolution inelastic neutron scattering study of the DBMH crystal [16] revealed that this group is a quasi-free rotor, which is contrary to the crude idea that the "big" bromine atoms will hamper the space around Me_2 and, thus, hinder its "rotation". Below 40 K, the INS spectra exhibit excitations at 14.7 and 24.6 cm^{-1} that were assigned to transitions between levels of same symmetry 0^A-1^A and 0^E-

1^E In the Raman spectra [18], scattered lines exist at 15.2 and 23.7 cm^{-1}. The fact that the intensities of these transitions are a function of time after freezing is another consequence of the quantum behavior of the rotor Me_2. Specifically this phenomenon is a consequence of the progressive departure of a part of the population with spin ½ into level 0^E to more stable O^A level (spin 3/2) via spin conversion. In section 2.2, it was indicated that the DFT calculations could not reproduce the Me_2 experimental conformation because, at equilibrium, the methyl group must always present only three PPD maxima as in Fig. 1b. These calculations were performed strictly using the Born-Oppenheimer approximation to the hydrogen nuclei without considering their spin states. Consequently, the energy states of the methyl groups in small hindering potentials must always be studied as solutions of the Schrodinger equation of a uni-axial quantum rotor.

6. Conclusion

6.1. An experimental study of the Raman and infra-red spectra of the fully hydrogenated 1,3-dibromo-2,4,6-trimethylbenzene (DBMH) at 288 K was presented. These spectra cover the range 80 - 3500 cm^{-1} with a resolution of approximately 3 cm^{-1}. Additionally, INS spectra were recorded in the same frequency range below 30 K. In parallel, quantum chemistry calculations of the molecular conformation and of the internal modes of vibration were performed. They consisted of DFT calculations using the MPW1PW91 functional with the LANL2DZ basis set augmented with polarization functions. The molecular equilibrium conformation that was calculated theoretically is very close to that obtained using neutron diffraction at 120 and 14 K with the exception of the Me_2 environment. The DFT calculations fail to produce the exact molecular conformation because they cannot consider the fact that Me_2 is a symmetrical “quantum rotor” with spin states. Nevertheless, these calculations provide an acceptable value for the rotation hindering barrier because they take into account the energy related to the spatial part of the Hamiltonian.

6.2. Using the geometry with P_{ring} as a symmetry plane as the equilibrium molecular geometry, a first calculation of the internal modes frequencies was performed assuming the harmonic approximation. The use of scaling factors of 0.983 for frequencies smaller than 1800 cm^{-1} and another factor equal to 0.958 for higher frequencies results in an agreement better than 1.5%. Furthermore, the values of the calculated intensities are qualitatively in agreement with those of the experimental peaks.

6.3. Another DFT calculation was performed using the same starting equilibrium conformation, but taking into account the anharmonicity of the motions. The agreement between calculation and experiment is now excellent for all of the frequencies below 1800 cm^{-1}, and the calculations

overestimate the C-H stretching modes in the range 2900-3200 cm^{-1} by less than 1.5 %. It is not necessary to use arbitrary scaling factors.

6.4. The contribution of internal vibrations to normal vibration potential energy (PED) was obtained within the harmonic approximation. Rocking, bending and stretching modes that are specific to internal methyl groups deformations during the vibration were localized and the calculations resulted in small differences in the frequencies of the Me_2 vibrations and those of Me_4 and Me_6. The specific excitations of the methyl torsion modes cannot be seriously calculated using DFT because this type of calculation neglects the spins of the methyl groups. Our previous INS studies [16, 17] demonstrated the necessity to take into account the quantum behavior of the methyl groups, particularly Me_2, which is subjected to a small hindering potential because of the symmetry of its environment.

Acknowledgements – This work benefited from the "Polish-French Polonium 2009-2010 program". S. Zeroual received financial support for her thesis work from the "PROFAS- Boursiers Franco-Algériens" program, and she thanks the "Laboratoire Sciences Chimiques de Rennes" for its hospitality. Thanks to Pr. R. Swietlik, Dr P. Roy, Dr. O Hernandez and Dr. M. Fourmigué for their helpful advices. The data from neutron diffraction or inelastic scattering have been collected thanks to LLB, ILL and ISIS.

References

[1] J. A. Draeger, Spectrochim.Acta A, 41A (1985) 607

[2] B. Bussian, H. Eysel, Spectrochim.Acta A, 41A (1985) 1149

[3] J. A. Pople,H. Schlegel, R. Krisnan, D. DeFrees, J. Binkley, M. Frisch, R. Whiteside, R. Hoot, W. Hehre, Int. J. Quantum Chem. Quantum Chem. Symp. 15 (1981) 269

[4] A. Scott, L. Radom, J. Phys. Chem., 100 (1996) 16502

[5] G. Rauhut, P. Pulay, J. Phys. Chem. 99 (1995) 3093

[6] J. Baker, A. Jarzecki, P. Pulay, J. Phys. Chem., 102 (1998) 1412

[7] D. Braden, B. Hudson, B. S. J. Chem. Phys., 104 (2000) 982

[8] Prager, M.; Heideman, A. Chemical Reviews, 97(1997) 2933

[9] Meinnel, J.; Häusler, W.; Mani, M.; Tazi, M.; Nusimovici, M.; Sanquer, M.; Wyncke, B.; Heidemann,A; Carlile, C.J.; Tomkinson, J.; Hennion, B. Physica B, 180 and 181 (1992) 711

[10] J. Meinnel, C. J. Carlile, K. S. Knight, J. Godard, Physica B, 226 (1996) 238

[11] J. Meinnel, H. Grimm, O. Hernandez, E. Jansen, Physica B, 350 (2004) E459

[12] F. Boudjada, J. Meinnel, A. Cousson, W. Paulus, M. Mani, M.Sanquer, Neutrons and Num. Methods A.I.P., CP479 (1999) 217

[13] A. Boudjada, O. Hernandez, J. Meinnel, M. Mani, W. Paulus, Acta Cryst. C, C57 (2001) 1106

[14] A. Boudjada, J. Meinnel, A. Boucekkine, O. Hernandez, M.T.Fernandez-Diaz, J.Chem. Physics, , 117 (2002) 10173

[15] J. Meinnel, A. Boudjada, A. Boucekkine, F. Boudjada, A. Moréac, S. F. Parker, J. Phys. Chem., 112 (2008) 11124

[16] J. Meinnel, B. Hennion, M. Mani, B. Wyncke, C. J. Carlile, Physica B, 213 and 214 (1995) 649

[17] M. Plazanet, M. R. Johnson, A. Cousson, J. Meinnel, H. P. Trommsdorff, Chem. Phys., 285 (2002) 299

[18] M. Plazanet, M. A. Neumann, H. P. Trommsdorff, Chem. Phys. Lett., 320 (2000) 651

[19] O. Hernandez, A. Cousson, M. Plazanet, M. Nierlich, J. Meinnel, Crystal Struc . Com., C59 (2001) o445

[20] M. J. Frisch, G. W. Trucks, H. B. Schlegel, G. E. Scuseria, M. A. Robb, J. R. Cheeseman, J. A. Montgomery, Jr., T. Vreven, K. N. Kudin, J. C. Burant, J. M. Millam, S. S. Iyengar, J. Tomasi, V. Barone, B. Mennucci, M. Cossi, G. Scalmani, N. Rega, G. A. Petersson, H. Nakatsuji, M. Hada, M. Ehara, K. Toyota, R. Fukuda, J. Hasegawa, M. Ishida, T. Nakajima, Y. Honda, O. Kitao, H. Nakai, M. Klene, X. Li, J. E. Knox, H. P. Hratchian, J. B. Cross, C. Adamo, J. Jaramillo, R. Gomperts, R. E. Stratmann, O. Yazyev, A. J. Austin, R. Cammi, C. Pomelli, J. W. Ochterski, P. Y. Ayala, K. Morokuma, G. A. Voth, P. Salvador, J. J. Dannenberg, V. G. Zakrzewski, S. Dapprich, A. D. Daniels, M. C. Strain, O. Farkas, D. K. Malick, A. D. Rabuck, K. Raghavachari, J. B. Foresman, J. V. Ortiz, Q. Cui, A. G. Baboul, S. Clifford, J. Cioslowski, B. B. Stefanov, G. Liu, A. Liashenko, P. Piskorz, I. Komaromi, R. L. Martin, D. J. Fox, T. Keith, M. A. Al-Laham, C. Y. Peng, A. Nanayakkara, M. Challacombe, P. M. W. Gill, B. Johnson, W. Chen, M. W. Wong, C. Gonzalez, and J. A. Pople, Gaussian, Inc., Pittsburgh PA, 2003. Gaussian 03, Revision B.04, Gaussian, Inc., Pittsburgh PA, 2008.

[21] D. A. Long, Raman Spectroscopy, McGraw-Hill: New York, 1977

[22] S. Shen, G. A. Guirgis, J. R. Durig, Struct. Chem., 12 (2001) 33

[23] D. Michalska, R. Wysokinski, Chem. Phys. Lett., 403 (2005) 211

[24] P. B. Nagabalasubramanian, S. Periandy, S. Mohan, Spectrochem. Acta Part A, 74 (2009) 1280

[25] N. Sundaraganesan, B. Anand, C. Meganathan, B. Dominic Joshua, Spectrochimica Acta Part A, 68 (2007) 561

[26] P. Wojciechowski, D. Michalska, Spectrochimica Acta Part A, 68 (2007) 948

[27] M. Karabacak, M. Kurt, A. Ataç, J. Phys. Org. Chem., 71 (2009) 321

[28] P. Wojciechowski, K. Helios, D. Michalska, Vibrational Spectroscopy, 57 (2011) 126

[29] V. Barone, J. Chem. Phys. 122 (2005) 014108

[30] V. Barone, J. Phys. Chem.. A, 108 (2004) 4146

[31] A. Daniel Boese, Jan M. Martin, J. Phys. Chem.. A, 108 (2004) 3085

[32] V. Barone, Chem. Phys. Lett., 383 (2004) 528

[33] V. Barone,G. Festa, A. Grandi, N. Rega, N. Sanna, Chem. Phys. Lett., 388 (2004) 279

[34] B. Wilson, D. C. Decius, C. Cross, Molecular Vibrations, Mc Graw Hill, N. Y. 1955

Figures captions

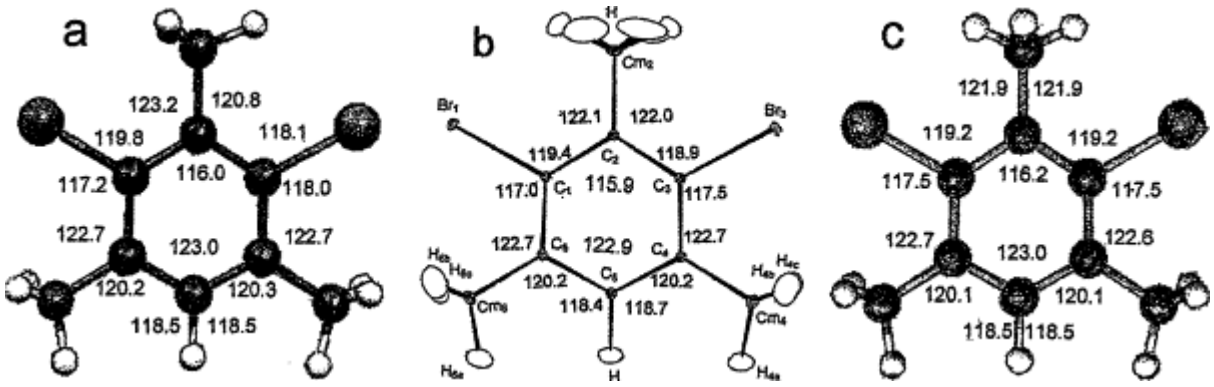

Fig. 1. Bond angles in the DBMH molecule: 1a- Optimized conformation using DFT computation; 1b- Obtained from neutron diffraction at 120 K; 1c- Conformation obtained from DFT calculations with the constraint that the plane perpendicular to the ring plane is a symmetry plane.

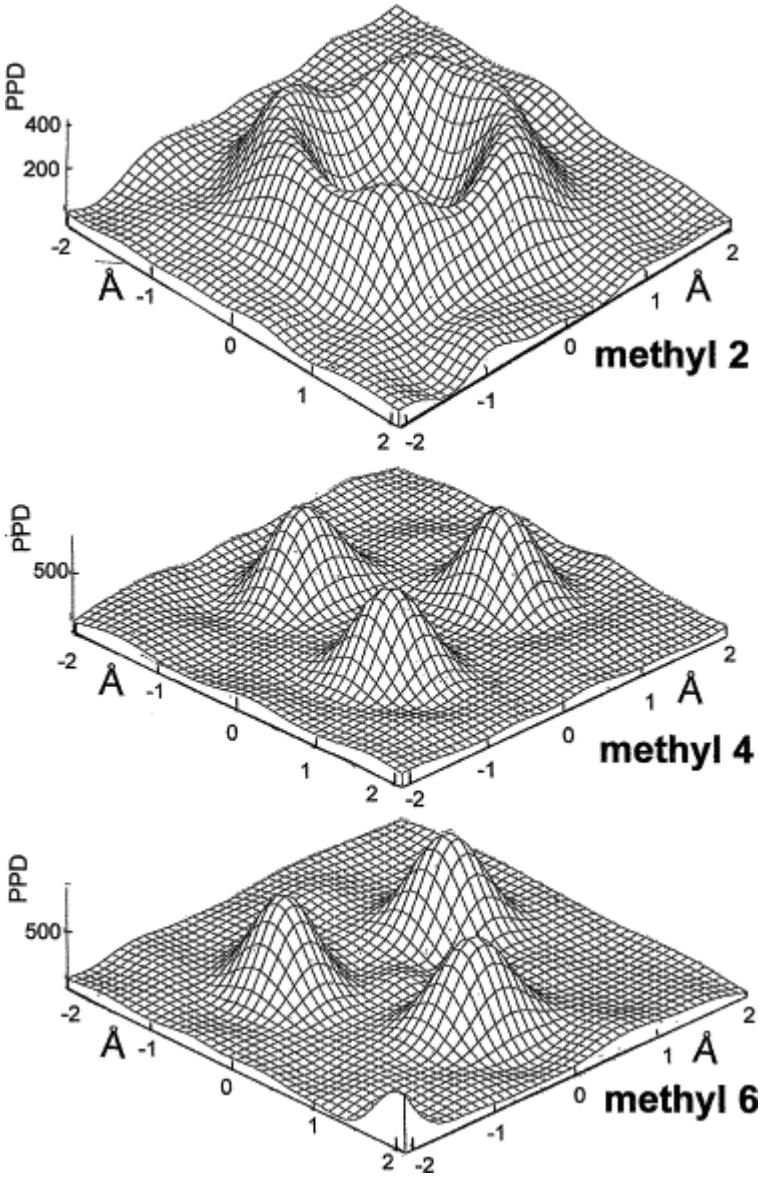

Fig. 2. Proton probability density for methyl groups Me_2, Me_4 and Me_6 obtained using neutron diffraction on a single crystal of DBMH at 120 K [18]. Each probability density graph is a cut in a plane perpendicular to the C_i-C_{mi} bond and containing the maxima of the PPD (i= 2, 4 or 6).

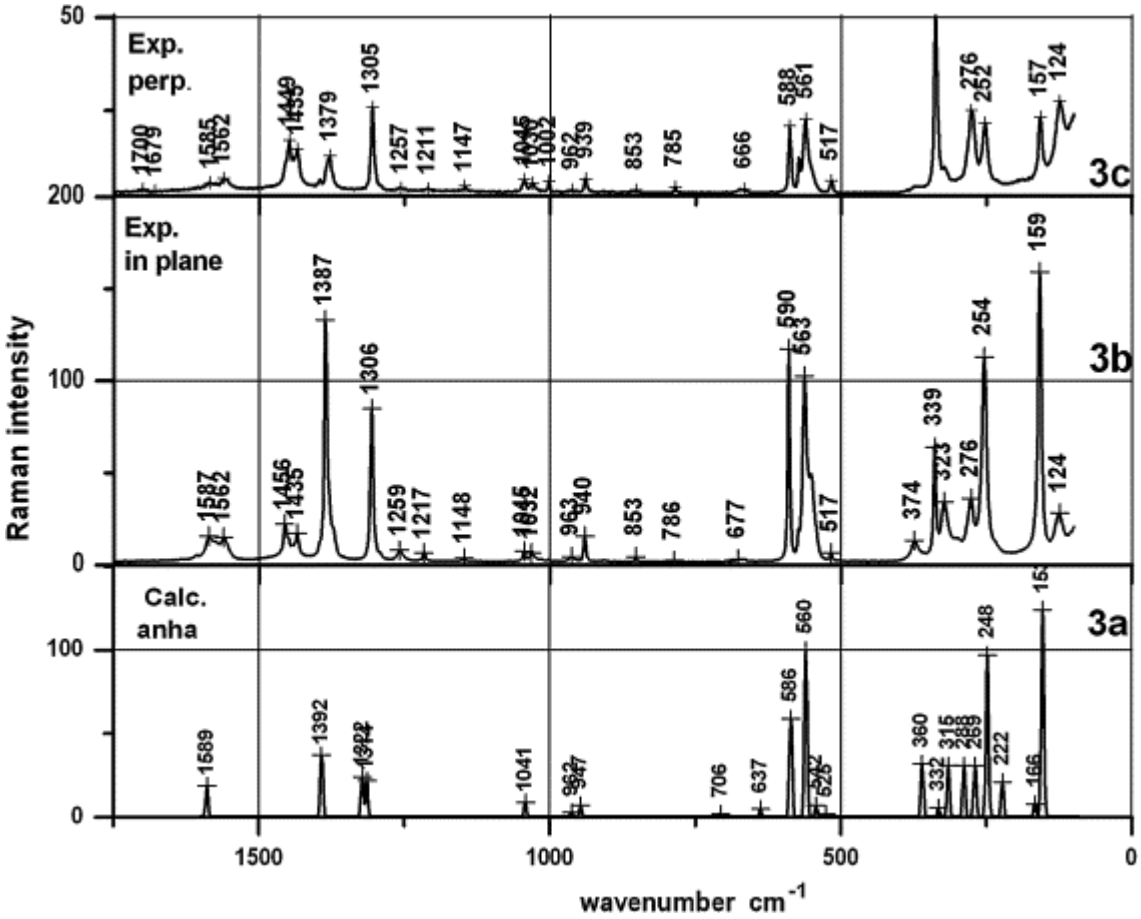

Fig. 3. DBMH Raman spectra: 3a- Calculated using DFT with the optimized conformation; 3b and 3c: Experimental spectra obtained at 288 K using excitation from an He-Ne laser line at 6328 Å, for 3b- the electric field E of the excitation beam was nearly in the molecular plane, for 3c- E was nearly normal to the molecular plane.

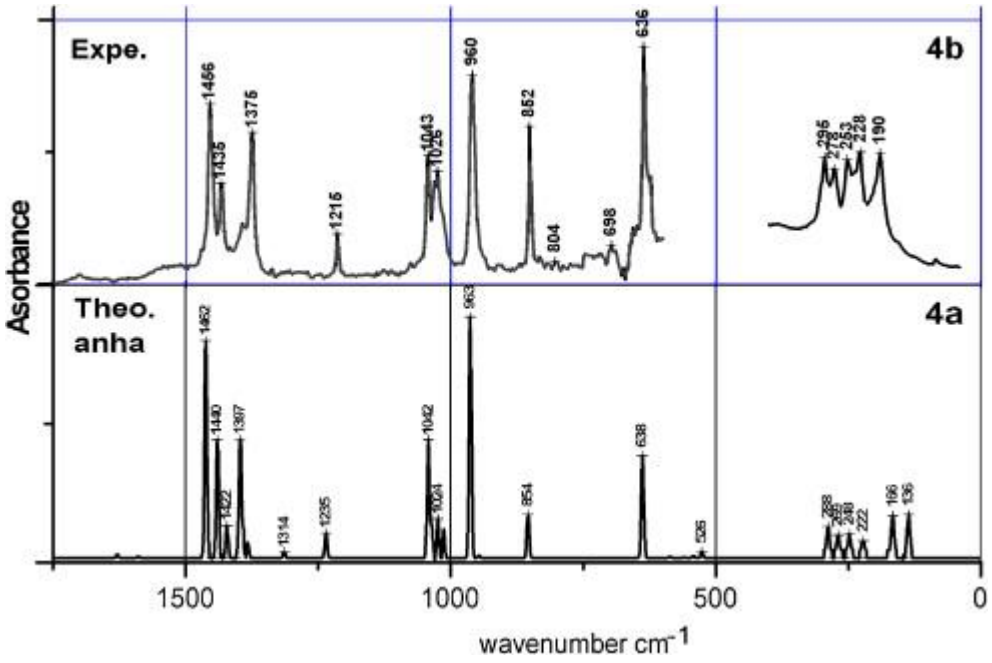

Fig. 4. DBMH infra-red absorption spectra: 4a- Calculated using DFT with the optimized conformation, 4b- In the range 500 - 1800 cm^{-1}, spectrum obtained using a Varian Fourier transform spectrometer; In the range100 – 400 cm^{-1} spectrum obtained on the AILES line using synchrotron radiation at SOLEIL and a Bruker Fourier transform spectrometer.

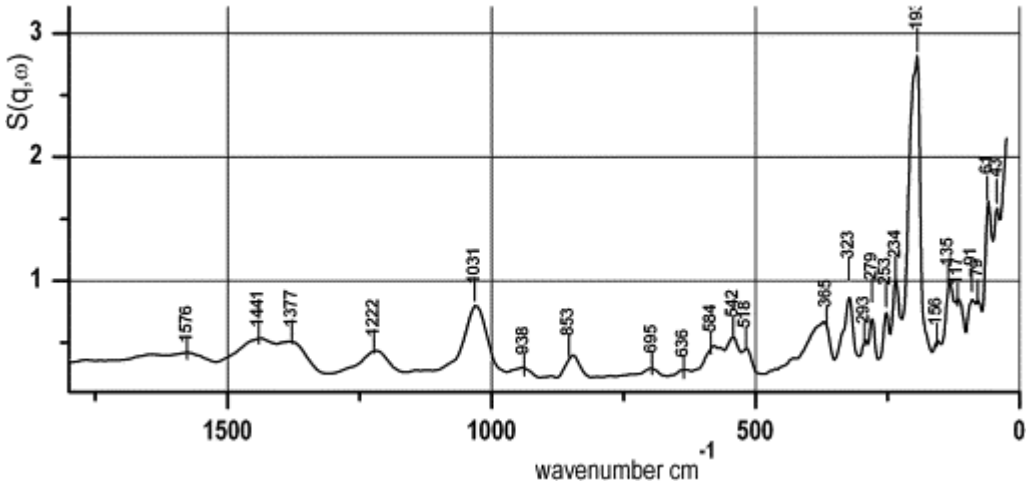

Fig. 5. Inelastic neutron scattering spectra which were obtained below 30 K using the TOSCA spectrometer at ISIS

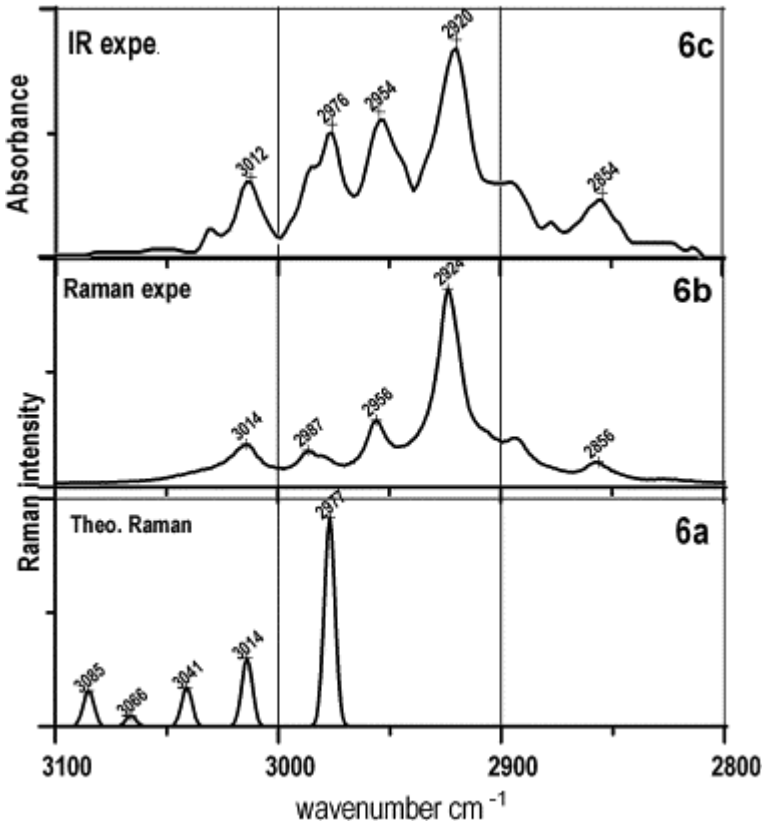

Fig. 6. Spectra in the 2800 - 3200 cm^{-1} range specific to the methyl groups stretching vibrational modes; 6a- DBMH Raman spectrum calculated by DFT; 6b- Raman experimental spectrum at 288 K; 6c- Infra-red experimental absorption at 288 K.

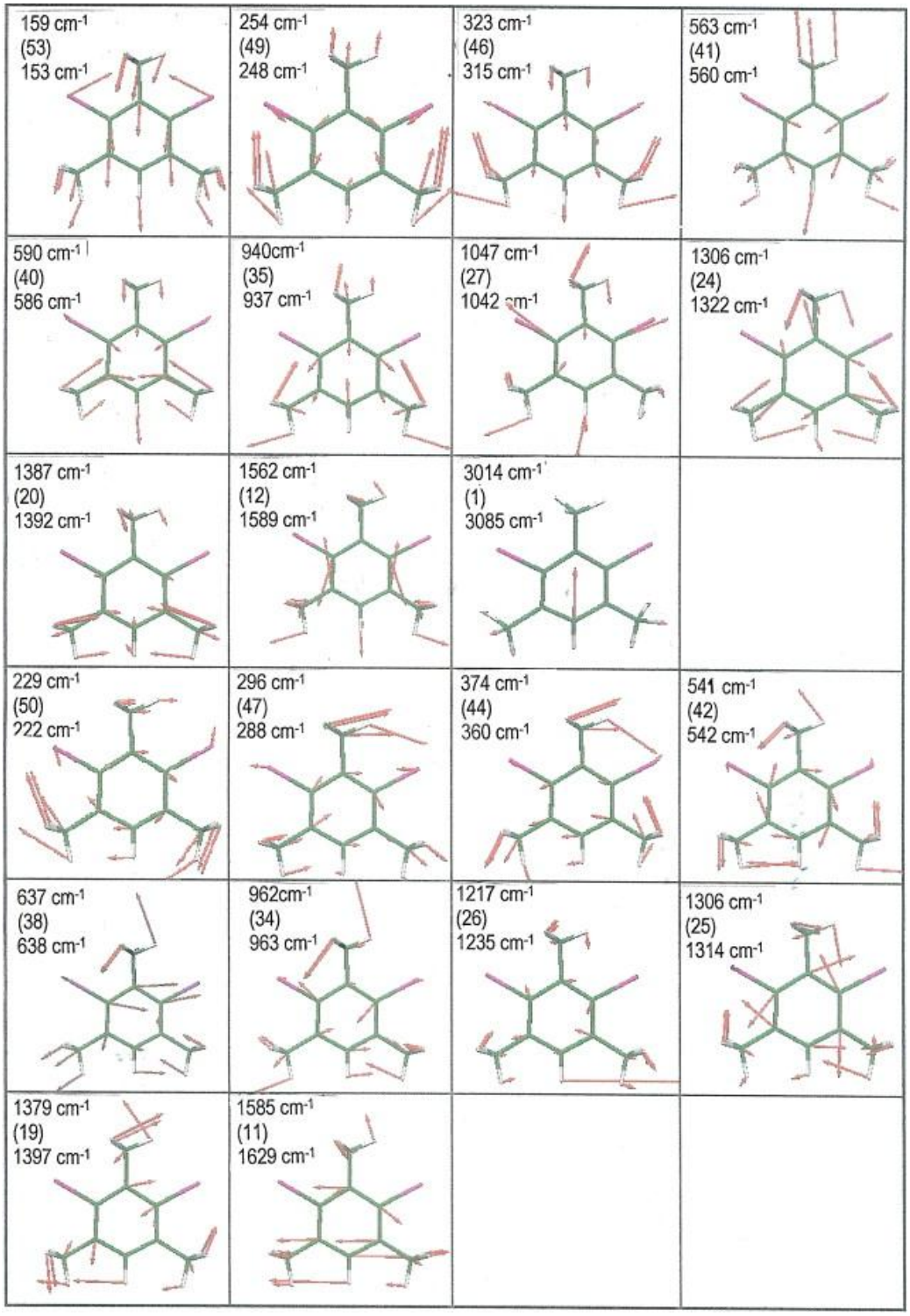

Fig. 7. Illustration of the atomic displacements for the twenty one "skeleton" in-plane vibrational modes (from DFT calculations): the first number at the top of each small figure corresponds to the frequency of an experimental observation (Raman or IR), the second (in parentheses) corresponds to the numbering from the highest frequency to the lowest, and the third number is the calculated anharmonic frequency.

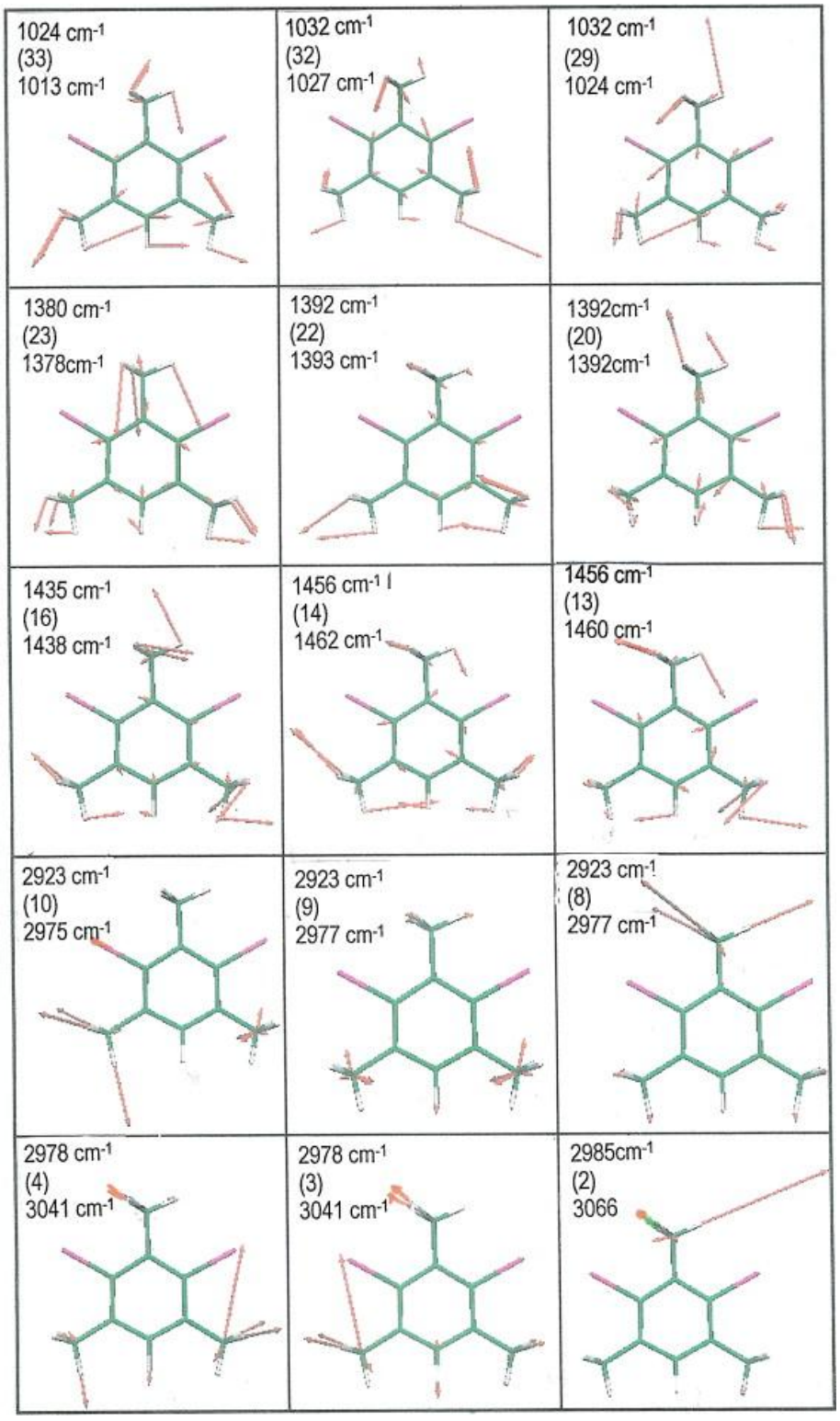

Fig. 8. Illustration of the atomic displacements for the fifteen in plane vibrational modes of “methyl groups” (from DFT calculations)

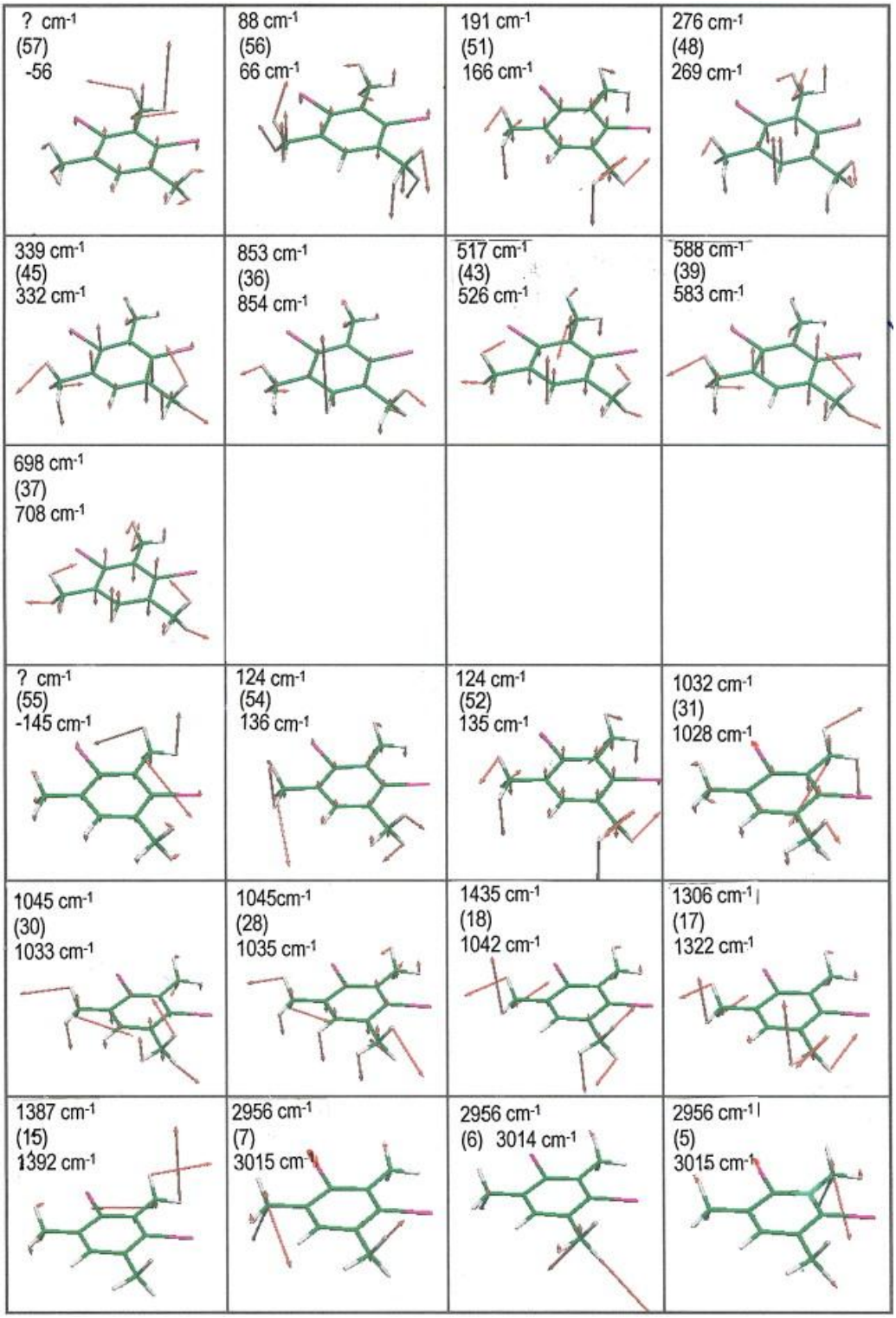

Fig. 9. Illustration of the atomic displacements for the nine "skeleton" and twelve"methyl groups" out of plane vibrational modes (from DFT calculations)

Tables

Table 1. Bond lengths and angles in DBMH. Column n° 2: neutron diffraction at 14 K, col. n° 3: neutron diffraction at 120 K, col. n°^{s} 4 and 6: DFT calculations with the MPW1PW91 functional and the LANL2DZ basis set augmented with polarization functions (the plane of symmetry is the benzenic ring plane for n° 4 and the plane perpendicular to the ring for n° 6), col. n° 5: basis set without polarization functions.

1	2	3	4	5	6
Distances Angles	Expe 14 K	Expe 120 K	Cal_1 P_{ring}	Cal_2 P_{perp}	Cal_3 P_{perp}
C_1-C_2	1.4025(19)	1.403	1.4061	1.4055	1.4058
C_2-C_3	1.4038(15)	1.399	1.4050	1.4108	1.4058
C_3-C_4	1.3962(14)	1.392	1.4030	1.4055	1.4012
C_4-C_5	1.3943(19)	1.391	1.3960	1.4030	1.3964
C_5-C_6	1.3939(15)	1.391	1.3968	1.4030	1.3964
C_1-C_6	1.3967(14)	1.392	1.3995	1.4055	1.4013
C_1-Br_1	1.9037(19)	1.898	1.9154	1.9645	1.9173
C_2-C_{m2}	1.4993(15)	1.497	1.5020	1.5068	1.5024
C_3-Br_3	1.9060(30)	1.904	1.9183	1.9645	1.9170
C_4-C_{m4}	1.5008(16)	1.498	1.5024	1.5067	1.5022
C_5-H_5	1.0911(16)	1.091	1.0864	1.0855	1.0864
C_6- C_{m6}	1.5000(20)	1.501	1.5019	1.5067	1.5022
C_6-C_1-C_2	123.60(5)	123.5	123.49	123.46	123.23
C_6-C_1-Br_1	117.06(9)	117.0	118.03	117.45	117.54
C_2-C_1-Br_1	119.34(9)	119.5	118.42	119.08	119.23
C_1-C_2-C_3	115.77(5)	115.9	116.27	116.00	116.24
C_1-C_2-C_{m2}	121.65(5)	122.1	120.46	122.00	121.94
C_3-C_2-C_{m2}	122.58(9)	122.0	123.27	122.00	121.82
C_2-C_3-C_4	123.59(9)	123.5	122.99	123.46	123.26
C_2-C_3-Br_3	119.02(4)	118.9	119.79	119.09	119.16
C_4-C_3-Br_3	117.39(4)	117.5	117.23	117.45	117.58
C_3-C_4-C_5	117.08(11)	117.2	117.31	117.09	117.14
C_3-C_4-C_{m4}	122.70(10)	122.6	122.71	122.88	122.74
C_5-C_4-C_{m4}	120.22(5)	120.2	119.98	120.03	120.12
C_4-C_5-C_6	122.87(5)	122.9	123.02	122.89	122.99
C_4-C_5-H_5	118.53(8)	118.7	118.50	118.55	118.50
C_6-C_5-H_5	118.60(11)	118.4	118.49	118.55	118.50
C_5-C_6-C_1	117.09(11)	117.1	116.93	117.09	117.14
C_5-C_6-C_{m6}	120.33(9)	120.2	120.31	120.03	120.12
C_1-C_6-C_{m6}	122.60(10)	122.7	122.76	122.88	122.74

Table 2. DBMH normal modes of vibration: Comparison of the experimental Raman (3), IR (4) and INS (5) bands with the theoretical anharmonic ω_{anh} (6), harmonic scaled ω_{hsc} (8) and harmonic ω_h (10) frequencies, Raman scattering activities (14), Raman intensities: calculated (15) and observed (16), IR absorption: calculated (17) and observed (18)

		Experimental frequencies ω cm^{-1}			Calculated frequencies ω cm^{-1}										Raman activity and intensities			IR absorption	
1	**2**	3	4	5	6	7	8	9	9b	10	11	12	12b	13	14	15	16	17	18
N°	*Sym* P_{ring}	ω_R *Raman*	ω_{IR} *IR*	ω_N *INS*	ω_{anh} cm^{-1}	*col.6 - col.3*	ω_{hsc} cm^{-1}	*col.8 - col.3*	*Ra/*ω_h cm^{-1}	ω_h cm^{-1}	*col.10 - col.3*	ω_{hp} cm^{-1}	*Sym* P_{perp}	*col.12 - col.10*	*Activity* Å^4/amu	I_{cal} *rel.*	$I_{R\,exp}$ *rel.*	$A_{cal.}$ km/mol	I_{IR} *exp.*
1	A’	3014	3012	3000	3085	71	3088	74	0,935	3223	209	3223	A’	0	94	33	17	10	9
2	A’	2987	2985		3066	79	3080	95	0,928	3215	230	3201	A"	-14	27	11	14	5	3
3	A’	2978	2976	2970	3041	63	3051	71	0,935	3185	207	3184	A’	-1	70	36	12	19	15
4	A’	2978	2976		3041	63	3050	72	0,935	3184	206	3184	A"	0	29			9	
5	A"	2956	2954		3015	59	3030	74	0,935	3163	207	3172	A’	9	52	63	26	6	18
6	A"	2956	2954		3014	58	3026	70	0,936	3159	203	3159	A’	0	33			11	
7	A"	2956	2954		3015	59	3026	70	0,936	3159	203	3159	A"	0	90			4	
8	A’	2924	2920	2925	2977	53	2961	38	0,946	3091	168	3087	A’	-4	157	193	97	8	20
9	A’	2924	2920		2977	53	2963	40	0,948	3082	159	3082	A’	0	344			16	

		Experimental frequencies ω cm^{-1}			Calculated frequencies ω cm^{-1}										Raman activity and intensities			IR absorption	
10	A’	2924	2920		2975	51	2962	39	0,948	3082	159	3082	A"	0	24			18	
11	A’	1587	-	1578	1629	42	1629	44	0,957	1657	72	1657	A"	0	33	28	15	1	2
12	A’	1562	-	1565	1588	26	1602	40	0,958	1630	68	1637	A’	7	21	19	15	0.5	2
13	A’	1449	1456		1460	11	1479	23	0,967	1505	49	1503	A"	-2	6			57	
14	A’	1456	1456		1462	6	1475	19	0,970	1501	45	1502	A’	1	5	23	22	38	66
15	A"	1435	1430		1422	-13	1465	16	0,972	1490	41	1491	A’	1	8			10	
16	A’	1435	1435		1438	3	1464	29	0,964	1489	54	1488	A"	-1	4			4	
17	A"	1435	1435	1441	1441	6	1459	24	0,967	1484	49	1484	A’	0	14	24	17	25	45
18	A"	1435	1435		1440	5	1458	23	0,935	1483	48	1483	A"	0	5			1	
19	A’	-	1397		1397	0	1417	30	0,935	1442	55	1439	A"	-3	0.4	4		30	25
20	A’	1387	1392	1392	1392	1	1407	30	0,936	1429	50	1429	A’	0	34	50		1	
21	A’	1387	1392		1393	6	1405	26	0,936	1424	37	1425	A’	1	5	20	131	7	57
22	A’	1387	1375	1377	1384	-3	1397	5	0,946	1420	33	1421	A"	1	7			3	
23	A’	1380	1375		1378	-2	1389	9	0,948	1413	33	1415	A"	2	4	4		4	
24	A’	1305	1313		1322	17	1330	25	0,948	1353	48	1351	A’	-2	20	30	84	0	5

		Experimental frequencies ω cm^{-1}			Calculated frequencies ω cm^{-1}										Raman activity and intensities			IR absorption	
25	A’	1305	1313		1314	8	1315	9	0,957	1338	32	1338	A"	0	9	22		2	
26	A’	1217	1215	1218	1235	18	1228	11	0,958	1249	32	1249	A"	0	1	1	6	6	20
27	A’	1047	1043	1045	1041	-6	1046	-1	0,967	1064	17	1064	A’	0	5.	9	7	30	45
28	A "	1045	1043		1035	-10	1043	-4	0,970	1061	14	1061	A’	0	2			7	
29	A’	1032	1028	1026	1024	-8	1041	9	0,972	1059	27	1058	A"	-1	0	2	6	6	32
30	A "	1045	1045		1033	-12	1040	-1	0,964	1058	13	1057	A"	-1	0.5			4	
31	A "	1032	1026		1028	-4	1033	1	0,967	1051	19	1054	A’	3	0			0	20
32	A’	1032	1024		1024	-8	1032	0	0,968	1050	18	1049	A’	-1	1			1	
33	A’	1015	1015		1013	-2	1019	17	0,935	1037	35	1038	A"	1	0.3	1	2	8	
34	A’	962	960		962	0	974	12	0,935	991	29	992	A"	1	1.7	3	4	61	76
35	A’	940	-	938	947	7	947	8	0,936	963	24	964	A’	1	3.40	7	5	0	
36	A"	853	852	853	854	1	870	17	0,936	885	32	885	A’	0	0.2	1	4	10	40
37	A"	-	-	695	706	11	720	22	0,954	732	34	731	A’	-1	0.7	2	-	0	7
38	A’	-	636	637	637	1	641	4	0,977	652	16	652	A"	0	1.2	5	-	26	52
39	A"	588	-	585	583	-5	584	-4	0,990	594	6	594	A"	0	2.8	68	116	0	2

		Experimental frequencies ω cm^{-1}			Calculated frequencies ω cm^{-1}										Raman activity and intensities			IR absorption	
40	A’	590	-		586	-4	582	-6	0,997	592	2	592	A’	0	11			0	
41	A’	561	-		560	-1	558	-3	0,991	568	5	568	A’	0	19	100	100	0	
42	A’	-	540	542	542	2	537	-7	0,991	546	6	548	A"	2	1.2	7	-	1	5
43	A"	517	517	518	525	9	532	15	0,956	541	24	539	A’	-2	0.3	2	6	2	11
44	A’	374	-	369	360	-14	362	-12	1,016	368	-6	377	A"	9	2.7	32	13	0	-
45	A"	339	-		332	-7	336	-3	0,988	342	3	342	A"	0	0.4	6	63	0	-
46	A’	323	-	323	315	-8	314	-9	1,013	319	-4	319	A’	0	2	31	34	0	-
47	A’	-	295	293	288	-7	285	-11	1,021	290	-6	303	A"	13	1.7	31	-	3	4
48	A"	276	276	279	269	-7	277	1	0,979	282	6	281	A’	-1	1.5	31	36	3	3
49	A’	252	253	253	248	-4	248	-4	1,008	252	0	252	A’	0	4	97	111	3	3
50	A’	-	228	234	222	-7	224	-5	1,004	228	-1	230	A"	2	0.7	21	-	2	4
51	A"	-	190	193	166	-24	185	-6	1,016	188	-3	188	A’	0	0.2	8	-	4	4
52	A"	124	-	135	135	11	165	-1	0,743	167	43	167	A"	0	0.3			4	-
53	A’	157	-	156	153	-4	156	-1	1,004	158,4	1	160	A’	2	2	124	136		1
54	A"	124	-	135	136	12	155	21	0,785	158	34	159	A’	1	0.1	34	25	4	-

		Experimental frequencies ω cm^{-1}			Calculated frequencies ω cm^{-1}										Raman activity and intensities			IR absorption	
55	A"	-	-	-	-145	?	117	-		119	-	81	A"	-38	0.3				-
56	A"	88	-	91	66	?	80	-8	1,086	81	-7	80	A'	-1	0.6				-
57	A"	21	-	-	-56	?	70	49	?	71	-	-94	A"	?	0.0				-

Table 3. The predominant components of the PED matrix (relative phases and % contributions) for the in-plane modes of vibration of DBMH

1	2	3	4	5	6	7	8
n°	ω_R cm^{-1}	% C_aX stretching %C_mH stretching	% -$C_aC_aC_a$- bending	% -C_aC_aX bending	% ring C_aC_a stretching	% $C_aC_aC_mH$ torsion	% C_aC_mH + HC_mH bending(χ_6,θ_6)
1	3014	67 s_5	14 α_5	-	(t_4 +t_5) (6)		
2	2987	48 r_{2a} – 30 (r_{2b} + r_{2c})		-	-		
3	2978	-8 r_{4a} +12 (r_{4b} + r_{4c}) - 35 r_{6a} +28 (r_{6b} + r_{6c})		-	-		
4	2978	-35 r_{4a} + 28 (r_{4b} + r_{4c}) + 8 r_{6a} +12 (r_{6b} + r_{6c})		-	-		
8	2924	20 r_{2a} – 66 (r_{2b} + r_{2c})					
9	2924	12 r_{4a} + 30 (r_{4b} + r_{4c}) + 14 r_{6a} +34(r_{6b} + r_{6c})					
10	2924	14 r_{4a} + 34 (r_{4b} + r_{4c})- 12 r_{6a} - 30 (r_{6b} + r_{6c})					
11	1587	4 s_2 + 7 (s_4 +s_6)	10 (α_1- α_3) - 14 (α_4-α_6)	15 β_5+ 3 β_2-5(β_1+β_3)	9 (t_1 -t_2+t_3)+16(t_4 - t_5+t_6)	-	18 (χ_2,θ_2 +χ_4,θ_4 +χ_6,θ_6)
12	1562	4 s_2	15(α_2+α_5) -15(α_1+α_3+α_4+α_6)	12(-β_1+β_3-β_4+β_6)	16(t_3 +t_6) -16(t_1 +t_2 +t_4 +t_5)	-	14 (χ_2,θ_2 +χ_4,θ_4 +χ_6,θ_6)
13	1456	-	-	- 6 β_5	4(t_2-t_5)	11η_2 + 15 η_6	- 18(χ_2,θ_2) + 23(χ_6,θ_6)
14	1456	-	-	4 β_5	-	- 6 η_2 + 19η_4+ 6 η_6	6 (χ_2,θ_2)-25 (χ_4,θ_4)+ 6(χ_6,θ_6)
16	1435	-	-	-	-	16 η_2+10 η_4+14 η_6	-16(χ_2,θ_2) + 10(χ_4,θ_4)- 14
19	1387	4 (s_1-s_3)	8(α_1- α_3)	4β_2 - 6β_5 -4(β_4 -β_6)	12 (-t_1+ t_2+ t_3 - t_4 - t_6)	-12 η_2+ 8η_4-7η_6	17(χ_2,θ_2)-11(χ_4,θ_4)+7(χ_6,θ_6)
20	1387	7 (s_4 +s_6)	6($\alpha_4$$\phi_4$+ $\alpha_6$$\phi_6$)- 6($\alpha_1$$\phi_1$+$\alpha_3$$\phi_3$+$\alpha_5$$\phi_5$)	-	4(t_4 +t_6)	- 18 (η_4+η_6)	8(-χ_2,θ_2)+21(-χ_4,θ_4)+26 (-χ_6,θ_6)
21	1387	- 5 s_2	2$\alpha_5$$\phi_5$- 2$\alpha_2$$\phi_2$	4(-β_1+β_3) +6(β_4 -β_6)	6 (t_1+t_2+t_3+t_6) – 6 (t_4+t_5)	25 (η_2-η_4+η_6)	18(χ_2,θ_2)- 6(χ_4,θ_4)+13(χ_6,θ_6)
22	1387	4 (s_4-s_6)	-	4 β_5	-	-5 η_2 +3 η_4- 8 η_6	33(χ_4,- θ_4) + 25(- χ_6, θ_6)
23	1380	-	-	10(β_1- β_3+β_4- β_6)	7 (t_1 +t_2 +t_3 -t_6)	5 η_2 - 8 η_4- 3 η_6	-32(χ_2,θ_2)+11(χ_4,-θ_4)+7(χ_6,-θ_6)

24	**1305**	$15\ (s_2 + s_4 + s_6)$	$-6(\alpha_2 + \alpha_4 + \alpha_6) + 6(\alpha_1 + \alpha_3 + \alpha_5)$	$-5(\beta_1 + \beta_3 + \beta_5)$	$-12\ (t_2 + t_4 + t_6)$	$8\ (\eta_4 + \eta_6)$	$31\ (\chi_2, \theta_2 + \chi_4, \theta_4 + \chi_6, \theta_6)$
25	**1305**	$-5\ (s_2 + s_4 + s_6)$		$15(\beta_1 - \beta_2 + \beta_3 - \beta_4 + \beta_5 - \beta_6)$	$33\ (t_1 - t_2 + t_3 - t_4 + t_5 - t_6)$	$22\ (\eta_2 + \eta_4 + \eta_6)$	$8(\chi_4, \theta_4) - 12\ (\chi_2, \theta_2 + \chi_6, \theta_6)$
26	**1217**	$4\ (s_1 - s_3) - 8\ (s_4 - s_6)$	-	$28\beta_5 - 4\ \beta_2 - 6(\beta_1 + \beta_3)$	$10\ (t_3 + t_4 - t_5 - t_6)$	$15\ (\eta_2 + \eta_4 + \eta_6)$	$-7(\chi_2, \theta_2) + 12\ (\chi_4, \theta_4 - \chi_6, \theta_6)$
27	**1047**	$12(s_1 + s_3) - 3(s_4 - s_6)$	$48(\alpha_1\phi_1 - \alpha_2\phi_2 + \alpha_3\phi_3 - \alpha_4\phi_4 + \alpha_5\phi_5 - \alpha_6\phi_6)$	-	$-6\ (t_1 + t_2 + t_3 + t_4 + t_5 + t_6)$	$10\ (\eta_2 + \eta_6)$	$9\ (\chi_2, \theta_2)$
29	**1032**	$8\ (s_2 - s_4)$	$6(-\alpha_1 + \alpha_2 - \alpha_3 + \alpha_4)$		$6\ (t_1 + t_2 - t_3 - t_4)$	$-27\ (\eta_2 + \eta_4)$	$19\ (\chi_2, \theta_2) - 16\ (\chi_4, \theta_4)$
32	**1032**	$8\ (-s_2 + s_4)$		$-3\ \beta_5$		$13\ (\eta_2 + \eta_4) + 18\ \eta_6$	$13\ (\chi_2 + \chi_4) + 17\ \chi_6$
33	**1015**	$6\ (s_4 - s_6)$		$+3\ \beta_5 + 2\beta_4$		$28(-\eta_2 - \eta_4) + 11\eta_6$	$-11(\chi_2, \theta_2) - 18(\chi_4\theta_4) + 13(\chi_6, \theta_6)$
34	**962**	$16\ (s_1 - s_3 + s_4 - s_6)$	$14\ (\alpha_1 - \alpha_3) + 7(\alpha_4 - \alpha_6)$	-	-	$15\ \eta_2 + 4\ \eta_4$	$19\ (\chi_2, \theta_2) + 6\ (\chi_4, \theta_4)$
35	**940**	$5\ s_2 - 6\ (s_4 + s_6)$	$5(\alpha_2\phi_2 - \alpha_4 - \alpha_6) + 8\alpha_5\phi_5 - 2(\alpha_1 + \alpha_3)$	$5(-\beta_1 - \beta_3 + \beta_4 + \beta_6)$	$8\ (-t_1 - t_2 + t_4 + t_5)$	$22\ (\eta_4 + \eta_6)$	$22\ (\chi_4 + \chi_6) - 8\ (\theta_4 + \theta_6)$
38	**637**	$22(s_1 - s_3) - 8(s_4 - s_6)$	$8\ (\alpha_1 - \alpha_3) + 10\ (\alpha_4 - \alpha_6)$	$6\ \beta_2 - 5\ \beta_5$	-	$6\ \delta_2$	$7\ (\chi_2, \theta_2)$
40	**590**	$8(s_1 + s_3) - 14(s_4 + s_6)$	$-8(\alpha_1 + \alpha_3) - 16\alpha_5\phi_5 + 28(\alpha_4 + \alpha_6)$	$-12(\beta_4 + \beta_6)$	-	$4\ (\eta_4 + \eta_6)$	$-5\ (\theta_4 + \theta_6)$
41	**561**	$11\ (s_1 + s_3) + 8\ s_2$	$10(\alpha_1\phi_1 + \alpha_3\phi_3) + 6(\alpha_4 + \alpha_6) - (11\alpha_2\phi_2 + 17\alpha_5\phi_5)$	$-10\ (\beta_4 + \beta_6)$	$13\ (t_2 + t_3 + t_4 + t_5)$	-	-
42	**541**	---	-	$16(\beta_1 + \beta_3) + 34(\beta_2 + \beta_4 + \beta_6)$	$4\ (t_1 - t_3)$	$16\ (\eta_2 + \eta_4 + \eta_6)$	$18\ (\chi_2 + \chi_4 + \chi_6)$
44	**374**	$11(s_1 - s_3) + 5(s_4 - s_6)$	-	$-16\ \beta_2 + 16(\beta_4 + \beta_6)$	$6\ (t_1 - t_2 + t_3 - t_6)$	$5\ \eta_2 - 7\ (\eta_4 + \eta_6)$	$-12\ (\chi_2 - \chi_4 + \chi_6)$
46	**323**	$14\ (s_1 + s_3)$	-	$6(\beta_1 - \beta_3) + 36(\beta_4 - \beta_6)$	$6\ (t_4 - t_6)$	$11\ (\eta_4 + \eta_6)$	$12\ (\chi_4 + \chi_6)$
47	**296**	$18\ (s_1 - s_3)$	$12(-\alpha_1 + \alpha_3) + 23(-\alpha_4\phi_4 + \alpha_6\phi_6)$	$18(\beta_1 - \beta_3) - 12\ \beta_2$	-	-	-
49	**252**	$22\ (s_1 + s_3)$	$-9(\alpha_1\phi_1 + \alpha_3\phi_3) + 12\ \alpha_2\phi_2 + 10\ \alpha_5\phi_5$	$-9(\beta_1 - \beta_3) - 20(\beta_4 - \beta_6)$	-	-	-
50	**229**	$11\ (s_1 - s_3)$	$6\ (-\alpha_1 + \alpha_3)$	$33(\beta_1 + \beta_3) - 21(\beta_4 + \beta_6)$	-	$5\ (\eta_4 + \eta_6)$	$6\ (\chi_4 + \chi_6)$
53	**159**	$14\ (s_1 + s_3)$	-	$52(\beta_1 - \beta_3) - 6(\beta_4 - \beta_6)$	$8\ (t_1 + t_2)$	-	-

Remark- the meaning of the symbols used is defined in the text (section 5.1)

Table 4. The predominant components of the PED matrix (relative phases and % contributions) for the out-of-plane modes of vibration of DBMH
Remark- the meaning of the symbols used is defined in the text (section 5.1)

1	2	3	4	5	6	7	8	9
n°	ω_R cm^{-1}	ω_{anha}	Me	% C_mH stretching	% $C_aC_aC_a$ bending o.p.	% C_aC_aX bending o.p.	% $C_aC_aC_mH$ torsion	% C_aC_mH + HC_mH bending
5	2956	3014	2	72 ($r''_{2b} - r''_{2c}$)				
6	2956	3015	6	16($-r''_{6b}+r''_{6c}$)+58($r''_{4b}- r''_{4c}$)				
7	2956	3015	4	56($r''_{6b} - r''_{6c}$) +16($r''_{4b} - r''_{4c}$)				
15	1435	1422	2				47 δ_2	10χ''_2 -33 θ''_2
17	1435	1441	4 + 6				28 δ_4 + 20 δ_6	5 χ''_4 +4 χ''_6 -20 θ''_4 -14 θ''_6
18	1435	1440	4 - 6				20 δ_4 - 29 δ_6	4 χ''_4 -5 χ''_6 -14 θ''_4 +20 θ''_6
28	1045	1035	4 + 6		12 (τ_3 - τ_4+τ_5 -τ_6)	-10(γ_4+γ_6) +9 γ_5	11δ_4 +14δ_6	7χ''_4 -10χ''_6 - 3θ''_6
30	1045	1033	- 4 + 6		15 (τ_3 - τ_4 -τ_5 +τ_6)	13 (γ_4 -γ_6)	-13 δ_4 +18 δ_6	13χ''_4 +4θ''_4+10χ''_6+3θ''_6
31	1032	1028	2		15 (τ_1 - τ_2)	9 γ_2 -6 (γ_1 +γ_3)	12 (-δ_4 +δ_6) + 24 δ_2	16χ''_2 +8 θ''_2 - 4χ''_6
36	853	856			10 (τ_4 - τ_5)	55 γ_5	12 (-δ_4 +δ_6)	9 (χ''_4 - χ''_6)
37	698	708			31(τ_1- τ_2 -τ_3 -τ_4 +τ_5 -τ_6)	11(κ_1-κ_2 +κ_3-κ_4 -κ_5) +8κ_5	22 (δ_4 +δ_6)	6 (χ''_2 - χ''_4 - χ''_6)
39	588	583			20(τ_1-τ_2+τ_3-τ_4+τ_5-τ_6)	21(γ_1-γ_3+κ_4-κ_5)	30 (δ_4 -δ_6) +8 δ_2	4 (-χ''_4 +χ''_6)
43	517	526			16(τ_1- τ_2 +τ_4 -τ_5)	28(γ_1+γ_2+γ_3 +γ_4+γ_6) - 8κ_5	-19 δ_2 +23(- δ_4 +δ_6)	-
45	339	332			16(τ_1- τ_3 -τ_4 +τ_6)	33(γ_1-γ_3 -γ_4 +γ_6)	36 (δ_2+δ_4 -δ_6)	-
48	276	270			4(τ_1- τ_2) - 6(τ_4 -τ_5)	30 (γ_1-γ_2+γ_3 -γ_4 -κ_5-γ_6)	–8 δ_2+ 13 δ_4 – 18 δ_6	
51	191	166			-	7 (γ_1+γ_2+γ_3)+ 12(γ_4+γ_6)	8 δ_2+ 35 δ_4 + 21 δ_6	
52	124	135	6	-			30 δ_4 + 57 δ_6	
54	124	136	4	-			– 16 δ_2 + 63 δ_4	
55	-	-145	2				82 δ_2	
56	88	66				-14 γ_1 +12 γ_3+11(κ_4-κ_5)	– 23 δ_2 + 12 δ_6	
57	21	-56				7 γ_1 + 9 γ_3	–53 δ_2+ 9 δ_4 – 7 δ_6	